Was the Little Ice Age more or less El Niño-like than the Medieval Climate Anomaly? Evidence from hydrological and temperature proxy data

Lilo M.K. Henke[1], F. Hugo Lambert[2], and Dan J. Charman[1]

[1]Department of Geography, College of Life and Environmental Sciences, University of Exeter, Amory Building, Rennes Drive, Exeter, UK, EX4 4RJ
[2]Department of Mathematics, College of Engineering, Mathematics and Physical Sciences, Harrison Building, Streatham Campus, University of Exeter, North Park Road, Exeter, UK, EX4 4QF

Correspondence to: Lilo Henke (lmkh201@exeter.ac.uk)

Abstract. The El Niño-Southern Oscillation (ENSO) is the most important source of global climate variability on interannual time scales and has substantial environmental and socio-economic consequences. However, it is unclear how it interacts with large-scale climate states over longer (decadal to centennial) timescales. The instrumental ENSO record is too short for analysing long-term trends and variability and climate models are unable to simulate past ENSO states accurately. Proxy data are used to extend the record, but different proxy sources have produced dissimilar reconstructions of long-term ENSO-like climate change, with some evidence for a temperature–precipitation divergence in ENSO-like climate over the past millennium, in particular during the Medieval Climate Anomaly (MCA; AD ∼800–1300) and the Little Ice Age (LIA; AD ∼1400–1850). This throws into question the stability of the modern ENSO system and its links to the global climate, which has implications for future projections. Here we use a new statistical approach using Empirical Orthogonal Function (EOF) based weighting to create two new large-scale reconstructions of ENSO-like climate change derived independently from precipitation proxies and temperature proxies respectively. The method is developed and validated using model-derived pseudoproxy experiments that address the effects of proxy dating error, resolution and noise to improve uncertainty estimations. We find no evidence that temperature and precipitation disagree over the ENSO-like state over the past millennium, but neither do they agree strongly. There is no statistically significant difference between the MCA and the LIA in either reconstruction. However, the temperature reconstruction suffers from a lack of high-quality proxy records located in ENSO-sensitve regions, which limits its ability to capture the large-scale ENSO signal. Further expansion of the palaeo-database and improvements to instrumental, satellite and model representations of ENSO are needed to fully resolve the discrep-

ancies found among proxy records and establish the long term stability of this important mode of climatic variability.

1 Introduction

25   The El Niño-Southern Oscillation (ENSO) is the most influential source of interannual variability in the modern climate. The 'warm' El Niño state is characterised by a weaker sea surface temperature (SST) gradient across the equatorial Pacific and a shift in precipitation from the western Pacific toward the central Pacific, while the 'cool' la Niña state is roughly the opposite. Although ENSO originates in the tropical Pacific, it has far-reaching effects through teleconnections on some regions
30   in higher latitudes, and El Niño years are generally anomalously warm on a global scale. However, it is unclear whether there is a link between anomalously warm or cool periods and the two ENSO states on decadal to centennial timescales. Given the severe socio-economic consequences of ENSO events (Hjelle and Glass, 2000; Page et al., 2002; Kovats et al., 2003; Badjeck et al., 2010), and a warmer future under continued anthropogenic warming, it is important to understand the 'natural'
35   long-term ENSO and its interaction with the climate. It allows for an evaluation of the effects of anthropogenic impacts on recent and future ENSO behaviour (Collins, 2005; Guilyardi et al., 2009; Vecchi and Wittenberg, 2010; Bellenger et al., 2014).

Recent multi-model studies of projected changes in ENSO under anthropogenic warming suggest robust changes to ENSO-driven temperature and precipitation, including an increase in extreme El
40   Niño (Cai et al., 2015a) and La Niña (Cai et al., 2015b) events, and changes in the ENSO SST pattern and ENSO-driven precipitation variability (Power et al., 2013). However, most current general circulation models (GCMs) cannot simulate many aspects of the modern day ENSO accurately, often overestimating the western extent of the Pacific Cold Tongue and failing to correctly simulate central Pacific precipitation anomalies, ENSO feedbacks, and ENSO amplitude (Bellenger et al.,
45   2014; Collins, 2005; van Oldenborgh et al., 2005).This translates into uncertainty over simulations of past ENSO-like climate change, calling for alternative sources of climatic information to supplement, complement and corroborate the model and instrumental data. This is done using proxy climate records such as treerings, tropical ice cores, sediment cores and corals (Jones and Mann, 2004).
50   There are very few annually-resolved proxy records available longer than ∼500 years (Mann et al., 2008). The issue with high-resolution proxies is that they tend to be short in length; trees and corals, for example, rarely live beyond a few centuries (Jones and Mann, 2004). Some such highly resolved records are available for the more distant past, but these generally offer snapshots rather than continuous records (McCulloch et al., 1996; Corrège et al., 2000; Abram et al., 2009).
55   However, there are several long, lower-resolution proxy records of ENSO variability on decadal to millennial scales, often derived from lake sediments (cf Conroy et al., 2010), marine sediments (cf

Barron and Anderson, 2011), or speleothems (cf Maupin et al., 2014). While these are unable to capture the interannual frequency and amplitude of individual ENSO episodes, they provide an insight into longer-term ENSO-like climate states and average ENSO behaviour. Although there are some endeavours to combine some low-resolution proxies, often to capture spatial gradients (Conroy et al., 2010; Yan et al., 2011b; Anderson, 2012), there has not, to our knowledge, been a comprehensive effort to systematically merge a large set of such low-resolution records to create a long-term reconstruction of ENSO-like climate variability. Doing this could shed light on the long-term stability of ENSO and its links with the wider climate, for example by examining ENSO behaviour under different dominant cool or warm climate states, which in turn can inform our understanding of potential future ENSO-like changes in a warmer world.

A number of proxy, instrumental and modelling studies investigate links between ENSO and global climate variability on interannual (Klein et al., 1999; Wang et al., 1999), decadal (Nelson et al., 2011), centennial (Mann et al., 2005; Trouet et al., 2012) and millennial (Cane, 2005; Ivanochko et al., 2005; Moy et al., 2002; Shin et al., 2006) time-scales. A wide range of proxy records and modelling studies point to substantial shifts in the ENSO-like state of the climate linked to changes in solar variability on orbital time-scales (Clement et al., 2001; Barron and Anderson, 2011), movement of the Intertropical Convergence Zone (ITCZ; Partin et al., 2007; Gomez et al., 2004; Carré et al., 2005; Nelson et al., 2011) and changes in ocean circulation linked to sea level rise (Wanner et al., 2008; McGregor et al., 2008). In the more recent past, changes in solar irradiance and stratospheric aerosol loadings due to volcanic activity have played significant roles in modulating the hemispheric to global scale climate (Mann et al., 2009). The so-called Medieval Climate Anomaly (MCA; ca. AD 800–1200) and the Little Ice Age (LIA; ca. AD 1300–1850 Yan et al., 2011b) were periods of anomalously warm and cool conditions respectively, at least in the Northern Hemisphere if not globally (Jones and Mann, 2004; Mann et al., 2009). Regarding ENSO-like behaviour however, proxy evidence for the past 2000 years appears to be more ambiguous. A range of proxies point to a more northerly ITCZ (Haug et al., 2001; Sachs et al., 2009; Tierney et al., 2010) during the MCA, which is characteristic of La Niña-like conditions and is in agreement with warming patterns found in multiproxy reconstructions of hemispheric and global scale temperature (cf Mann et al., 2009). Langton et al. (2008) similarly infer a reduction in El Niño-like activity during the MCA based on ocean basin ventilation changes in Indonesia. In contrast, a Southern Oscillation Index reconstruction based on two proxy records (Yan et al., 2011b) shows an El Niño-like state during the MCA and a La Niña-like LIA. This seems to be supported by a number of other precipitation proxies from the West Pacific (Yan et al., 2011a) and East Pacific (Moy et al., 2002). Other precipitation proxies indicate a highly variable ENSO during the LIA, including two multidecadal droughts in Java (Crausbay et al., 2006), high amplitude rainfall fluctuations in Madagascar (Brook et al., 1999), and three southerly ITCZ excursions (Haug et al., 2001).

These discrepancies in long-term ENSO-like variations between proxy records raise two important questions. The current dynamical understanding of ENSO is underpinned by the strong relationship between temperature and rainfall observed today, and the relationships between the ENSO 'source region', the tropical Pacific, and teleconnected regions, which largely fall between 40°S and 40°N. As Yan et al. (2011b) highlight, however, temperature and precipitation proxies appear to disagree on the ENSO-like states of the MCA and the LIA. To what extent, therefore, does the modern-day precipitation–temperature relationship in the source and teleconnected regions continue to exist in the past? The second question concerns the relation of ENSO to the wider climate; is there a link between global temperatures and long-term ENSO state on multidecadal to centennial time-scales? A comparison between the MCA and the LIA can give some insight into this, and may hold some clues to what we can expect under anthropogenic climate change.

The use of proxy archives can contribute valuable insights on past climate variability by extending the instrumental records back in time, but substantial uncertainties remain. This is because all reconstructions have inherent limitations and ambiguities that must be identified and dealt with appropriately. These include resolution, dating errors, noise, limited and/or skewed spatial coverage, and nonlinear responses to the climatic variable of interest (Jones et al., 2009). Various statistical techniques have been employed to create multiproxy reconstructions of climatological phenomena, broadly falling into the categories 'composite plus scaling' (CPS) or 'climate field reconstruction' (CFR) (Jones et al., 2009). CPS encompasses any method which involves combining standardised proxy records into a single reconstruction which is subsequently calibrated to a known timeseries of the target variable (e.g. instrumental temperature record) to provide a quantitative estimate of the variable. CFRs, on the other hand, aim to reconstruct large-scale spatial patterns of climatic change using covariance between proxies and instrumental data. Within both methods there is a wide variety of approaches; see Jones et al. (2009) for detailed descriptions and examples of both CPS and a range of CFR methods. The focus of this study – comparing the climate signals in temperature and precipitation proxy records separately – calls for a slightly different approach.

Here we create two new ENSO reconstructions, one derived from temperature proxies and one from precipitation proxies, using a new method for assessing the stability of the modern-day ENSO patterns in the source region and the wider teleconnected regions. In a fashion similar to e.g. Braganza et al. (2009), proxy records are not tuned to instrumental data other than a simple location-dependent weighting. While this precludes direct quantitative comparisons, it removes the bias towards high-frequency trends that stems from calibrating to the relatively short (∼150 year) instrumental record (or indeed any short record; Cook et al., 1995; Jones and Mann, 2004). The method amplifies the ENSO component of proxy records and simultaneously attempts to quantify uncertainty related to noise and incomplete spatio-temporal data coverage, whilst maximising the use of a wide range of tropical proxies. With this, we aim to answer two questions:

1. Do temperature and precipitation proxies show consistent long-term ENSO behaviour over the last millennium?

2. Do the LIA and the MCA differ significantly in their mean ENSO state?

Section 2 provides a description of the proxy and instrumental/reanalysis data used in this study and a concise overview of the methodology is given in Sect. 3. The results and discussion of the findings are presented in Sects. 4 and 5 respectively before revisiting the research questions and making concluding remarks in Sect. 6.

2 Data description

2.1 Proxy records

For this study, a comprehensive effort was made to collect all published proxy precipitation and temperature records between 40°S – 40°N that cover the last 2000 years. The large majority of records were accessed from the NOAA Paleoclimatology and Pangaea Databases (https://www.ncdc.noaa.gov/data-access/paleoclimatology-discussion/datasets). In addition, over 200 treering records were taken from the dataset used by Mann et al. (2008), and hence were subject to their criteria including length, intra-site signal coherence and sample density (see Appendix A for details). A set of coral records was taken from the dataset made available by Tierney et al. (2015); these were largely temperature proxies although some were assigned as precipitation proxies or excluded altogether based on information in the original publications (see Appendix A for details).

After collection, all records were screened for a maximum dating error of 60 years. Although somewhat arbitrary, this cut-off was decided by taking double the averaging binwidth of 30 years that was applied to the data prior to analysis (Appendix B3). This is a step towards addressing the issue of dating uncertainty while allowing a wider range of proxies to be utilised. Proxies with larger dating errors generally have lower (multi-annual to multi-decadal) resolution but are usually also much longer, and are arguably more useful for capturing long-term trends which may be less evident or reliable in annual-resolution proxies (cf Cook et al., 1995; Esper et al., 2002; Mann et al., 2008, on low-frequency trends in treerings). Other quality judgements regarding temporal resolution, record length and proxy location are accounted for by the method set out in Sect. 3 and Appendix B.

2.2 Modern climate datasets

Instrumental climate data are the best available in terms of dating accuracy, calibration and physical basis (Jones and Mann, 2004). However, their spatial coverage is not complete and sharply decreases back in time. The nature of the method used in this study calls for full spatial coverage over a long period; therefore, reanalysis products are more suitable. These are combinations of instrumental and satellite data interpolated using models. The 20th Century Reanalysis Version 2c (20CRv2c) is the

longest global dataset of atmospheric circulation available, spanning AD 1851-2014. It is based on surface pressure, temperature and sea ice distribution data, filled in with a 'deterministic' Ensemble Kalman Filter (EKF). It has a spatial resolution of 2°latitude $\times$ 2°longitude $\times$ 24 vertical pressure levels, and a temporal resolution of up to 6 hours. It has been demonstrated that the 20CRv2c is competent at representing the global tropospheric circulation as well as the mean state and variability of the hydroclimate – for a detailed description and evaluation of the product see Compo et al. (2011). The monthly mean surface air temperature and precipitation rate datasets were downloaded from the NOAA/OAR/ESRL PSD web site (http://www.esrl.noaa.gov/psd/). The 20CRv2c data were regridded to 2°$\times$3° to be comparable to the model data described below (Sect. 2.3). The climatology (for the period 8151-2012) was removed to produce monthly anomalies, which were then averaged to annual resolution.

2.3   General circulation model simulations

There are several comprehensive modelling projects with the aim of improving comparability between general circulation models (GCMs) produced by different teams. GCMs taking part in these projects perform a set of simulations with standardised forcings and boundary conditions. For this study, the pre-industrial control (piControl; pre-1850 parameters, no external forcings) and historical (AD 1850– 2000) runs from the Coupled Model Intercomparison Project 5 (CMIP5; Taylor et al., 2012) were used, in addition to the last millennium (past1000; AD 850–1850) runs from the Paleoclimate Model Intercomparison Project 3 (PMIP3; Braconnot et al., 2011, 2012). Of the six GCMs which have all three runs available, two were chosen for their similarity to 20CRv2c in terms of spatial ENSO representation (see Appendix B2) for precipitation (climate modelling groups in brackets):

- CCSM4 (National Center for Atmospheric Research)

- GISS-E2-R (NASA Goddard Institute for Space Studies)

  And two for temperature:

- IPSL-CM5A-LR (Institut Pierre-Simon Laplace)

- BCC-CSM1-1 (Beijing Climate Center, China Meteorological Administration)

All model datasets were regridded to 2°$\times$3°, converted to anomalies and degraded to annual resolution to enable comparison between models and with 20CRv2c.

3   Methodology

The method used in this study consists of two stages: first, a temperature and a precipitation ensemble of proxy networks is created based on GCM-derived pseudoproxy experiments; then, these network

6

ensembles are used to produce two independent reconstructions of ENSO-like climate change using the real proxy data weighted by temperature and precipitation ENSO patterns from 20CRv2c reanalysis data. This approach attempts to take into account the effects of proxy selection, the temporal limitations of individual proxies, and non-climatic noise. A brief overview of the method is given here, with a more extensive description in Appendix B.

3.1 Pseudoproxy creation

Pseudoproxies are simulated proxies that attempt to mimic various sources of uncertainty inherent in the real proxy records. This ranges from adding white Gaussian noise with a prescribed signal-to-noise (SNR) ratio to approximate non-climatic random noise, to more sophisticated process-based additions that take into account effects such as dating error, nonlinear and multivariate responses of the proxy sensor to the climate variable, and sampling biases (Mann, 2002; Smerdon, 2012). The utility of any pseudoproxy exercise lies in the fact that the answer to the question is known, as it can be derived directly from the original model dataset. By putting the 'signal plus noise' pseudoproxies through a method to make a reconstruction of the signal, it allows for inferences about the stability and limitations of the method, estimates of uncertainties due to noise and other proxy record characteristics and, as highlighted by the method used here, it provides a way of objectively and systematically selecting the most appropriate data (see Smerdon, 2012, for an introduction to pseudoproxy experiments).

Ideally, all pseudoproxies in this study would be created from proxy system models (PSMs; e.g. Dee et al., 2015). Unfortunately, many proxies (e.g. $\delta^{18}O$ from corals or speleothems) would require isotope-enabled GCMs which are not available for the model runs used in this study. treering widths (TRW), however, can be easily simulated using the VSLite Model, which is a freely available PSM desgined to estimate TRW based on minimal climatic input (Tolwinski-Ward et al., 2011; Breitenmoser et al., 2014; Evans et al., 2014). It is a simplified version of the full Vaganov-Shashkin model (Vaganov et al., 2006; Anchukaitis et al., 2006; Vaganov et al., 2011) and only requires temperature, precipitation and latitude information. All TRW records in the proxy dataset used in this study were thus represented using VSLite derived pseudo-TRW series. For the rest of the proxies, the GCM raw temperature or precipitation series were used.

White gaussian noise was added to all model temperature, precipitation and TRW series. Where the original publications (or in the case of the coral records, Tierney et al., 2015)) provided an indication of the strength of the proxy–climate relationship (e.g. R-value), the SNR was calculated. For all other records, a prescribed signal-to-noise ratio (SNR) of 0.4 (which corresponds to an R-value of $\sim$0.38) was used, as this has been shown to be a realistic average (Smerdon, 2012). The median calculated SNR was 0.79 for precipitation and 0.57 for temperature, suggesting the prescribed SNR of 0.4 is a conservative estimate. The pseudoproxies were also degraded to reflect the length, timespan and resolution of the real proxies.

3.2 Network ensemble creation

The creation of a network ensemble was done using a calibration-validation scheme to assess the ability of various pseudoproxy combinations to reconstruct multi-decadal ENSO-like precipitation or temperature variations over the past millennium. As 20CRv2c only covers ∼160 years, it is not suitable for testing over these timespans and the past1000 runs from GCMs were used instead. To account for the fact that the ENSO patterns in GCMs are different from the pattern in 20CRv2c (and the real ENSO pattern is likely to be different again), two different GCMs are used for the calibration and validation stages. This means the sensitivity of the networks to the shape of the ENSO-like pattern is tested. GCM selection is described in Appendix B2. The precipitation and temperature calibration GCMs (GCM$_{cal}$) were CCSM4 and ISPL-CM5A-LR, respectively; the corresponding validation GCMs (GCM$_{val}$) were GISS-E2-R and BCC-CSM1-1.

Using the GCM$_{cal}$ past1000 dataset, a thousand proxy networks were created via an 'add-one-in' pseudoproxy algorithm that automatically builds a network based on how much each proxy improves the reconstructive power of the network (Figure 1). Similar to a forward stepwise regression procedure, GCM$_{cal}$-derived pseudoproxies are gradually added to a 'base' network of zero proxies, testing the quality of the network with each addition, until all proxies have been incorporated (Fig. 1 a&b). The final 'optimal' network is that which performed best over all steps (Fig. 1 c). By repeating the process 1000 times adding different random noise series to the pseudoproxies each iteration, it addresses the influence of stochastic processes on the ability of a proxy network to optimally reconstruct the large-scale ENSO pattern.

The reconstruction process itself is a weighted average approach, where the proxy weights are based on the ENSO-like EOF pattern of the GCM$_{cal}$ past1000 run (for the add-one-in network building) or 20CRv2c (for the final reconstruction). First, all (pseudo-)proxies in the network were normalised to a common period of at least 100 years (see Sect. 3.3) and transformed using an inverse transform sampling (ITS; Emile-Geay and Tingley, 2016) to approach a normal distribution. The EOF values W at the proxy locations i were scaled such that their absolute sum at each timestep t is 1 (Equation B3). This EOF scaling deals with the fact that the number of proxies available changes over time, preventing more proxy-dense periods from getting amplified. Each proxy series P was then weighted by its corresponding (scaled, time-variable) EOF value Wn_P. Finally, the n weighted proxy series Pw were summed to create a single reconstruction series $ENSO_r$ (Equation B4. This is essentially a 'sparse' reconstruction of the PC, which is the dot product of the full raw dataset and EOF. The quality of a network was assessed by comparing $ENSO_r$ with the PC using the Pearson rank correlation R (see Appendix B4).

Validation was performed in two steps. First,the 1000 networks produced with the GCM$_{cal}$ were used to make reconstructions using GCM$_{val}$ past1000 data and the GCM$_{cal}$ EOF. Using data from a different GCM ensures complete separation between the calibration and validation periods, and tests the sensitivity of the networks to the spatial stability of the EOF pattern, as the ENSO-like

8
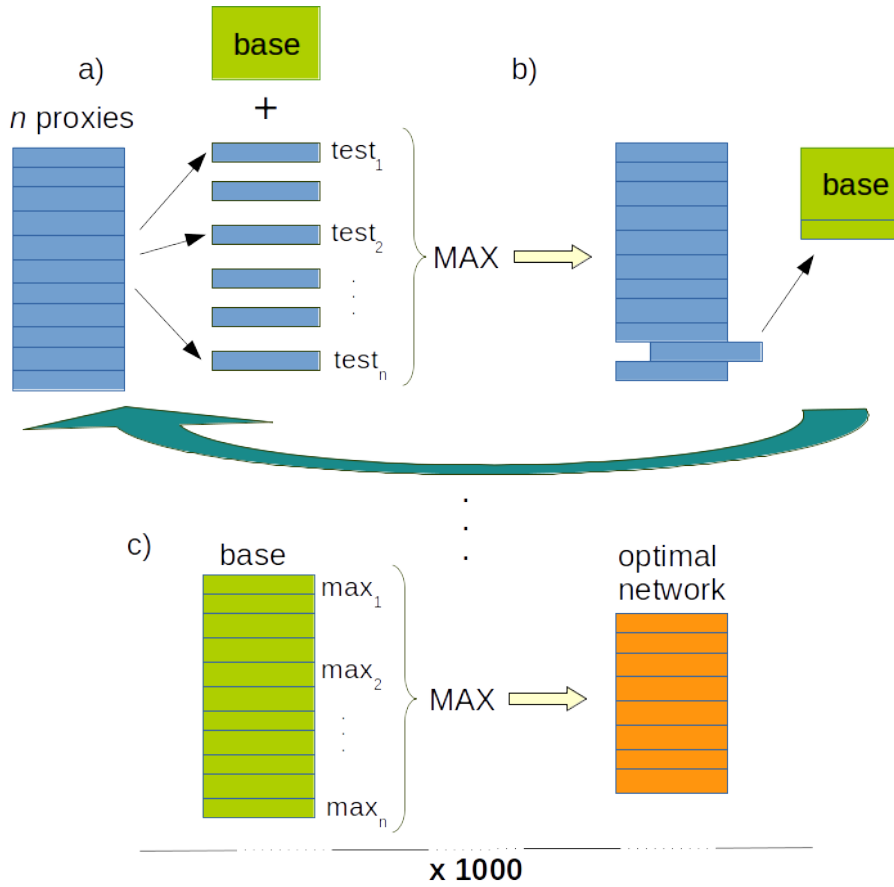
Figure 1. Network creation process diagram. Overview of the network creation process. a) A new network is created from the base network (*base*) plus each pseudoproxy individually, and tested for its reconstructive power. This results in n test scores; b) the highest score (max_n) is selected and the associated proxy is moved from the test-proxies to *base*. This is repeated until all test-proxies are incorporated into *base*. c) The 'optimal' network is selected by cutting *base* where max_n was highest. The entire process is repeated 1000 times, with new noise realisations being added to the pseudoproxies at the start of each run.

EOF from each model and from 20CRv2c is different. The switch from GCM_{cal} to GCM_{val} thus mirrors the switch between the GCMs and 20CRv2c. Each network was reconstructed 1000 times using GCM_{val} pseudoproxies, again adding different noise realisations for each iteration. Validation test scores were calculated to check the quality of these validation reconstructions compared to the validation PC (calculated using EOF_{cal} and GCM_{val} past1000 data). Second, critical values for the validation test scores were calculated by repeating the first validation step but using the GCM_{val} piControl run. If the validation R-value of a network failed to exceed R_{crit}, its reconstruction was deemed to be no better than random noise and was consequently discarded.

9

3.3 Final reconstruction

The remaining networks were used to create an ensemble of $ENSO_r$s using the real proxy data. The proxy records were first normalised to account for the different units (Equation B2) and subjected to an ITS transform, before undergoing the same reconstruction process used in the network creation. All ensemble members ($ENSO_r$) were then re-normalised to the reference period 0-650 yrBP to ensure comparability. The final ENSO reconstruction was taken as the ensemble mean, while the ensemble range represents part of its uncertainty envelope.

The last step in creating the reconstruction was calculating the final error range. Root mean square errors (RMSEs) were calculated for each network during validation, providing 1000 error estimates for each ensemble member. The 95th percentile for each member was calculated from this, and added and subtracted from the $ENSO_r$ series to find the maximum and minimum error limits. The uncertainty envelope around the final ENSO reconstruction (i.e. the ensemble mean) is thus a combination of the reconstruction ensemble range and the error ranges for individual ensemble members.

3.4 LIA-MCA difference analysis

The absence of a known reference period to which the reconstructions can be calibrated precludes any absolute comparison of the result with recent trends. However, it is possible to ascertain whether the MCA and the LIA differ significantly in how 'El Niño-like' they are. Evaluating the LIA-MCA difference directly also removes the bias introduced by taking any reference period (Mann et al., 2009). To do this, the means over the two periods were taken and the MCA mean subtracted from the LIA mean. If the difference is significantly greater than zero, the LIA is more El Niño like than the MCA; if the difference is significantly less than zero, the MCA is more El Niño-like than the LIA.

4 Results: ENSO reconstructions

The final ENSO reconstructions for precipitation and temperature and their proxy network density are shown in Figs. 2 and 3. The final number of networks included in the precipitation ensemble is 1000, of which 999 are unique (Fig. 2a). The total number of proxies used is 48, with a maximum of 40 for a single network. Proxy availability increases steadily throughout time, save a slight drop off in the most recent period (Fig. 2b). Although there is spread in the ensemble, there are clear peaks and troughs visible. The within-ensemble coherence was tested by correlating 1000 randomly chosen pairs with each other. This confirmed that there is generally good agreement over the full period (100-1500 yrBP) as well as during the MCA and LIA individually (Fig. 4).

The temperature reconstruction ensemble consists of 617 optimal networks, all of which are unique (Fig. 3a). The within-ensemble correlations are lower than for precipitation in the LIA though

still positive, and there is no distinct trend visible in the reconstruction. The total number of proxies used is 267, with a maximum of 116 for a single network. Despite the higher number of proxies available for temperature, the median proxy coverage (Fig. 3b black line) is lower compared to the precipitation reconstruction; while roughly the most recent 1000 years of the precipitation reconstruction are based on a median of 8 or more proxies, this is only true for the last ∼450 years of the temperature reconstruction. The steep increase in Fig. 3b. reflects the high number of treering and coral series, all but a handful of which are less than 600 years long (cf Mann et al., 2008; Tierney et al., 2015) and most of which are clustered in North America. The add-one-in method has mitigated some of the risk of co-varying, non-white noise in a subset of the proxies skewing the resulting reconstruction; testing showed that when all North American treering records were added to the reconstruction, a regional non-ENSO trend obscured the ENSO signal (not shown). However, the relatively poor spatial coverage elsewhere and the lack of long proxies leaves the reconstruction prone to spurious noise-driven trends in the earlier period. Unlike the precipitation ensemble, the temperature ensemble members vary quite widely among them, particularly in the early period (Fig. 4). Nevertheless, for both temperature and precipitation the error from proxy noise is overshadowed by the uncertainty associated with the choice of network – the ensemble spread makes up the bulk of the uncertainty envelope.

Figures 5 and 6 shows the proxy locations plotted onto the precipitation and temperature EOF patterns, respectively. The proxies included in the precipitation ensemble members are well-distributed over the western and eastern side of the Pacific, though missing good coverage of the central Pacific. The relatively uniform size of the bubbles suggests that there is no immediate preference of any one proxy over the others. The spatial distribution of the temperature proxy locations, in contrast, is highly skewed towards North America (Fig. 6), where most of the treering records are located, and again the central Pacific lacks coverage. The combination of this poor spatial coverage, low temporal coverage (Fig. 2b) and wide ensemble range (about double that of precipitation) leads to the expectation that the temperature reconstruction is of lower quality than the precipitation reconstruction. There is no clear preference of any combination of proxies, with most proxies being selected equally often (i.e. equal bubble sizes). The fact that the similarity of the EOF patterns of GCM_{cal} and GCM_{val} to the 20CRv2c EOF pattern was lower for temperature than for precipitation (Appendix. B2) further reduces confidence in the temperature reconstruction.

Figures 5 and 6 illustrate the benefit of using the pseudoproxy approach in creating the 'optimal' networks. There is no direct correlation between proxy weighting (indicated by the bubble colour) and frequency of use, suggesting that other aspects such as resolution, length and the relationship to other proxy locations played a significant role in determining the usefulness of a proxy which would be difficult to judge from the outset. The fact that the choice of proxy network is the dominant source of error is further evidence of the utility of the pseudoproxy 'optimal' network method. The high clustering of temperature treering records in North America is an example of where the add-

11

one-in method has worked to reduce the risk that some co-varying, non-white noise in a subset of the proxies skews the resulting reconstruction; testing showed that when all North American treering records were added to the reconstruction, a regional non-ENSO trend obscured the ENSO signal (not shown).

4.1 Comparing precipitation and temperature

Figure 7 shows the range of LIA-MCA differences for the individual members within the precipitation and temperature ensembles. The precipitation interquartile range indicates the LIA is more El Niño-like than the MCA, though the difference is statistically insignificant ($p = 0.22$). For temperature, there is no evidence of any difference between the ENSO-like state of the MCA and the LIA, with a median value very close to 0 ($p = 0.48$). There are also many more outliers (i.e. values outside the the 95% confidence interval) compared to precipitation, again reflecting the high uncertainty on the temperature reconstruction.

Figure. 8 shows the correlation between 1000 randomly chosen combinations of temperature and precipitation ensemble members as an indication of the agreement between the two climate variables. There is no correlation – positive or negative – apparent between the temperature and the precipitation reconstructions, neither over the entire 1500 years nor over the MCA or LIA individually. Whether this is a true physical phenomenon or simply a reflection of the high uncertainty on the reconstructions is difficult to separate. Therefore, it is not possible to categorically determine a systematic difference between the ENSO signals in temperature and precipitation proxies.

The definitions of the MCA and the LIA used here are based on those given by Yan et al. (2011b); there are many alternative definitions, however (Jones and Mann, 2004). To test the sensitivity of the results to the definition of these periods, we recalculated the LIA-MCA difference using two widely used alternative definitions: from Mann et al. (2009) (MCA = AD 950–1250, LIA = 1400–1700) and the Intergovernmental Panel on Climate Change (IPCC) Fifth Assessment Report (MCA = AD 950–1250, LIA = 1450–1850; Masson-Delmotte et al., 2013, , Fig. 9). For precipitation, the difference between the two period is more pronounced for the alternative definitions, with a weakly significantly more El Niño-like LIA ($p < 0.1$). For temperature there is very little change; although the median is negative for the alternative definitions, the interquartile range still encompasses zero. The precipitation reconstruction thus suggests that the LIA was more El Niño-like than the MCA, but our conclusion that there is no evidence for any precipitation–temperature correlation stands.

5 Discussion

An important question addressed in this study is whether the modern-day links between ENSO-like temperature and precipitation persist back in time. There is no concrete evidence in this study of any correlation between the precipitation and temperature reconstructions, whether positive (as in

12

380   the modern day) or negative (as suggested by Yan et al., 2011b). This is contrary to expectations based on instrumental and modelling data, which both show a strong relationship between ENSO-like precipitation and temperature. To test the robustness of the ENSO-like temperature–precipitation coupling in GCMs, we calculated the correlation between the temperature and precipitation ENSO-like EOF timeseries (PCs) in the six CMIP5 GCMs listed in Appendix B2. Four of the six models

385   show a significant ($p < 0.05$) positive precipitation–temperature correlation over the study region (40°S – 40°N) at annual and 30-year resolution for the historical run ($0.74 \leq R^2 \leq 0.98$), and five out of six for the past1000 run ($0.30 \leq R^2 \leq 0.92$; not shown). This is similar to coupling in the 20CRv2c data ($R^2 \geq 0.76$). The fact that the palaeodata apparently does not display this relationship over the past two millennia (cf Yan et al., 2011b, and this study) is thus interesting from a physical

390   dynamical point of view as it contradicts our conventional understanding of long-term ENSO-like climate change.

    There is also no evidence in the two reconstructions presented here that there was any significant difference in the mean ENSO-like climate state during the MCA and the LIA. This is also contrary to the findings of Yan et al. (2011b). They create a SOI reconstruction (SOI_{pr}) from two precip-

395   itation proxies from the Galápagos (Conroy et al., 2008) and the Indo-Pacific Warm Pool (Oppo et al., 2009), weighting them according to the relationship of local rainfall to the instrumental SOI. Interestingly, SOI_{pr} shows broad trends opposite to the precipitation reconstruction presented here, with a more La Niña-like LIA compared to the MCA. While the two proxies used were considered for this study, they were both rejected due to high dating errors (average around 100 years). Several

400   other precipitation (Tierney et al., 2010; Yan et al., 2011b) as well as temperature (Conroy et al., 2010) proxies supporting conclusions of the Yan et al. (2011b) study were similarly rejected due to high dating errors, as were proxies supporting the opposite conclusion (Partin et al., 2007; Conroy et al., 2009). Testing showed that applying the method described here using only the two proxies used by Yan et al. (2011b) produced highly similar results to their SOI reconstruction, suggesting it

405   is not a methodological difference but rather related to proxy selection. A reconstruction based on only two (poorly dated) proxies is likely to be more vulnerable to spurious noise or other climatic influences distorting the signal, as is evidenced by the degradation back in time of the reconstructions presented in this study as the number of proxies declines. This highlights the need for more accurately dated proxy records, which remains an issue for low-resolution but long proxy archives

410   such as marine sediments (Jones and Mann, 2004).

    A number of other (non-temperature or precipitation) ENSO-sensitive proxies that were not included in our reconstructions provide evidence for a more La Niña-like climate state in the MCA compared to the LIA, although the mean state of the LIA appears inconsistent. Sedimentary sterol concentrations in marine sediment off the Peru coast Makou et al. (2010) suggest the MCA coin-

415   cides with a reduction in El Niño activity, with both El Niño and La Niña activity increasing from the late MCA onwards. Based on a range of North American proxies Graham et al. (2007) conclude

that the MCA was characterised by arid conditions in western North America consistent with a La Niña-like state, followed by a wetter LIA. A basin ventilation record from the Western Pacific Warm Pool (WPWP) (Langton et al., 2008) agrees particularly well with the earlier part of our precipitation reconstruction. It shows a peak in El Niño activity at ∼1150 yrBP and a distinctive minimum during the MCA, followed by a more El Niño-like LIA characterised by a steady decline in activity. This decline is not apparent in our reconstruction, but is reflected in some other multi-millennial proxy records (Moy et al., 2002; Stott et al., 2004; Conroy et al., 2008).

Most multi-proxy reconstructions of ENSO variability are temperature-based, and focus on NINO regions. A NINO3 region (90°W–150°W and 5°S–5°N) temperature reconstruction by Mann et al. (2009) shows a slow millennial-scale warming trend (to a more El Niño-like state) from AD 1100 onwards, with relative cooling during the MCA compared to the LIA consistent with a La Niña-like state during the MCA. In contrast, Emile-Geay et al. (2013b) are unable to detect a systematic difference between the MCA and LIA in their Boreal winter NINO3.4 (120°W–170°W and 5°S– 5°N) SST reconstruction, which is consistent with the findings of this study. The discrepancy between the two ENSO reconstructions may be due to the difference in proxy networks, particularly the use of lower-resolution proxies here and by Mann et al. (2009) which contribute a substantial part of the signal, due to the slightly different definition of the NINO regions, or the target season (Boreal winter versus annual). Other reasons may be related to the methodology or target instrumental dataset, particularly for low-frequency variability and amplitude. Work by Emile-Geay et al. (2013b) indicates that the results of many temperature reconstruction methods are sensitive to the target SST dataset used for calibration, and Wang et al. (2015) find that the La Niña-like pattern in the MCA evident in Mann et al. (2008) is not a robust feature across CFR methods. The fact that multi-proxy reconstructions are less likely to show strong differences between the ENSO-like state of the MCA and the LIA again highlights the potential sensitivity of individual records to non-physical trends, and suggests that conclusions drawn from single proxy records must be considered with caution.

An issue not addressed in this study is the role of different 'flavours' of ENSO patterns. A different type of ENSO pattern, first defined by Ashok et al. (2007) and dubbed ENSO Modoki, differs from the traditional ('canonical') ENSO pattern in the shift of postive SST anomalies from the western Pacific (mainly in NINO3 and NINO3.4) to the central Pacific (NINO4; 170°W–120°W and 5°S–5°N), and its mid-latitude teleconnections. It is sometimes defined as the EOF2 of detrended SST data (note that the data in this study was not detrended, hence here it would be EOF3 Ashok et al., 2007; Cai et al., 2015a, b), or a combination of EOF1 and EOF2 (Takahashi et al., 2011; Karamperidou et al., 2015). Some modelling studies suggest that ENSO Modoki will increase in frequency compared to canonical ENSO as a result of anthropogenic climate change (Yeh et al., 2009; Kim and Yu, 2012; Cai et al., 2015a, b), and there is some model evidence that ENSO Modoki was also more common in the mid-Holocene (Karamperidou et al., 2015). The difference in equatorial spatial pat-

tern and teleconnections has implications for the interpretation of the proxy reconstructions in this study, as ENSO Modoki-like climate change may appear here as a reduction in ENSO-like activity.

455 The poor quality of the temperature reconstruction, which limits the statistical robustness of the precipitation–temperature comparison, is likely due to the low number and unequal distribution of available data locations. Most temperature proxies are located in teleconnected regions outside the ENSO source region, which have been shown to be subject to more temporal variability in precipitation–temperature relationships (Wilson et al., 2010; Coats et al., 2013; Gallant et al., 2013;

460 Lewis and LeGrande, 2015). A multi-region treering reconstruction of ENSO variability displays substantial variability in the strength of ENSO teleconnections over time and space (Li et al., 2013). The authors find that the Pacific Northwest and Texas-Mexican regions show highly unstable teleconnections (although there is no discussion on whether this is related to the different ENSO flavours). This may explain the lack of signal in the temperature reconstruction presented here, as many of

465 the temperature proxies are located in these teleconnected regions (Fig. 6). If the strength of the teleconnection has indeed changed over time, the weightings based on modern-day ENSO patterns would not reflect this; thus this reconstruction should be regarded as an indication of change of the modern-day ENSO-like climate pattern only. Without proxies located in the centre of action or more robustly teleconnected areas, the loss of signal due to unstable teleconnections can be expected to be

470 substantial as suggested by the results presented here.

An interesting observation of the EOF maps presented here (Fig. 5 and 6) is the low to no correlation between EOF weighting (bubble shading) and how often proxies are used (bubble size). Correlations of temperature proxy frequency of occurrence versus GCM-derived and 20CRv2c-derived EOF weighting are 0.23 and 0.20, respectively ($p < 0.05$); there is no significant correlation for

475 temperature proxies ($p > 0.54$). Two possible explanations for this are i) the climatic noise in the high-occurrence but low-weighted areas is less spatially correlated with the noise elsewhere than in the low-occurrence but higher weighted areas; or ii) the length and resolution of the proxy records have a more important effect on a proxy's utility than its weighting. For instance, the proxies off the Australian coast and in the west Pacific islands are mostly short (< 500 years) coral records; while

480 several of them have high weighting, their frequency of occurrence is very low. The proxy at the southern tip of Australia, in contrast, is a ~ 3600 year long treering record, and is the most frequently used temperature proxy. Overall, however, temperature proxy length is only very weakly correlated to occurrence frequency ($R = 0.17, p < 0.05$). The SNR assigned to the temperature pseudoproxies is similarly only very weakly correlated to frequency ($R = 0.13, p < 0.05$). In the precipitation case,

485 neither length nor SNR are significantly correlated to how often the proxies occur in the ensemble. The selection process is likely driven by a combination of these factors rather than any single factor, and is modulated by the number of proxies available. More detailed analysis will be needed to elucidate this.

15

There is some evidence that ENSO modulates the Pacific Decadal Oscillation (Yuan Zhang et al., 1997) on multidecadal timescales over the intrumental period (Newman et al., 2003) and further back in time (Verdon and Franks, 2006). The PDO is an SST anomaly pattern resembling ENSO located in the extratropical North Pacific (20°N – 45°N). Comparison of the precipitation reconstruction in this study with a reconstruction of the PDO over AD 993–1996 (MacDonald and Case, 2005) shows a slight tendency for the precipitation and PDO series to have the same sign over the MCA and LIA separately, although the relationships are not statistically significant (not shown). There is no indication of any relationship between the PDO and the temperature reconstructions, despite the fact that many of the temperature proxies are located in potentially PDO-sensitive areas (most notably North America). MacDonald and Case (2005) find a strongly negative PDO during the MCA (roughly equivalent to a La Niña-like spatial pattern), which corresponds to the qualitatively La Niña-like tendency of the precipitation reconstruction presented here. While there may be some conflation of ENSO and PDO signals in the reconstructions due to the similarity of their spatial patterns, it is not possible to distinguish these signals here. Moreover, the lack of correlation with the PDO reconstruction suggests the reconstructions presented here are distinct from the PDO. D'Arrigo and Wilson (2006) find no significant correlation between the 9-year smoothed reconstruction of the Asian expression of the PDO (based on East Asian treerings as opposed to the often-used North American treerings) and Boreal winter NINO3 SST, suggesting the ENSO-PDO link may be spatially variable.

5.1 Reflections on the method

The method set out in this study is one of few which attempt to take into account the effect of real spatial *and* temporal patterns of proxy records, thus increasing our confidence in their ability to accurately evaluate the effectiveness of the networks. To our knowledge, this is the only study in which realistic temporal proxy resolution has been taken into account by the pseudoproxies, in addition to their length. This is an improvement of the pseudoproxy design used by, for example, (Wang et al., 2014), who take into consideration the declining proxy availability back in time but not their resolution. The authors find that this already significantly impacts the quality of multi-proxy reconstructions, so the inclusion of proxy resolution as done here is likely to have further impacts. More extensive research is needed to quantify this however.

The 'optimal' network creation still has scope for improvement. Although we have screened for maximum dating errors, its effect on the included proxies is not explicitly assessed. This issue is often neglected in (multi) proxy reconstructions (but see Comboul et al., 2014, for a recent effort to address it systematically). Moreover, the noise simulation used here is relatively simplistic; the use of a wider noise spectrum (including red, and possibly even blue, noise) may alter the composition of the networks (Smerdon, 2012, and references therein). However, the issue remains that there is no easy way to determine the real noise spectrum of the proxies. With the advent of more isotope-

525 enabled GCM simulations, further improvement could come from the use of proxy system models to estimate more accurately the proxy-climate relationships (cf Conroy et al., 2008; Evans et al., 2013; Russon et al., 2013; Stansell et al., 2013; Steinman et al., 2012; Sturm et al., 2010; Thompson et al., 2011; Tierney et al., 2011; Dee et al., 2015).

The choice of dataset from which to derive an EOF is also a source of uncertainty (cf Emile-
530 Geay et al., 2013b), as differences in the EOF pattern will affect the weighting of the proxies. This is particularly pertinent for the precipitation reconstruction, as the modern-day ENSO precipitation signature is much less well-established than for temperature due to less and lower quality instrumental data. This is partially tested by using different GCMs to calibrate and validate the proxy networks. However, the true ENSO-like pattern has been non-stationary over time, as has been shown to be true
535 in 20CRv2 for the NAO and Pacific North American (PNA), for example (Raible et al., 2014). We tested the stability of the 20CRv2c temperature EOF used in this study by recalculating it for a running 30-year window and found substantial variability in the spatial pattern and amount of variance captured by the EOF. Further investigation is necessary to explore whether this result is an artefact of internal variability, is due to uncertainties in the reanalysis dataset, or reflects real changes in the na-
540 ture of ENSO. Nevertheless, it highlights the vulnerability of the majority of ENSO reconstructions (including ours) to the assumption that the modern-day ENSO is a good analogue for the past.

6   Conclusions

Two reconstructions of ENSO-like climate change are presented, based on temperature- and precipitation-sensitive proxies respectively. The quality of the reconstructions degrades further back in time as
545 there is less proxy data available, which is particularly detrimental to the temperature reconstruction. The main implications of these reconstructions are:

1. We find no evidence that temperature and precipitation proxies disagree over the ENSO-like state of the climate during the past two millennia. The two reconstructions in fact show little to no correlation, which is surprising as there is a strong relationship between temperature and
550 precipitation ENSO behaviour at interannual timescales in instrumental/reanalysis data and GCMs.

2. The precipitation reconstruction shows a tendency for a more El Niño-like LIA compared to the MCA, but the difference is not statistically significant and is not apparent in the temperature reconstruction. This result is insensitive to the choice of definition for the MCA and
555 LIA.

3. A major limitation on our ability to accurately reconstruct ENSO-like climate change back in time is the lack of high-quality, long proxy records in the tropical and subtropical latitude bands, and we reiterate the need for continued efforts to collect such data. The discrepancies

17

between the two series presented here and many other interannual and (multi-)decadal ENSO reconstructions are more likely to be reconciled with denser proxy networks in the ENSO source region, along with resampling of existing locations to increase the signal to noise ratio (Wang et al., 2014). The pseudoproxy experiments described in this paper can quite easily be adapted to search for optimal locations from which additional proxy information would be the most beneficial, as previously done specifically for corals by Evans et al. (1998) (see also Comboul et al., 2015, for a recent endeavour).

4. A final caveat is the reliance on modern-day ENSO patterns and the implicit assumption of its stationarity through time. Continued improvements in the ability of GCMs to accurately simulate and reproduce ENSO behaviour in conjunction with more high-quality proxy data will give both the palaeocommunity and the modelling community an increasingly reliable foundation for creating, calibrating and evaluating palaeo-ENSO reconstructions.

Appendix A: Proxy data details

Tables 1 and 2 provide an overview of the proxy records collected for this study. Where a proxy was rejected, the reason is given. 'AOI' refers to a proxy not being selected for any networks by the 'add-one-in' algorithm. This could be due to poor ability to capture the EOF pattern related to location or time resolution. Records from the NOAA Paleoclimate Database are identified by original publications. Where there are multiple timeseries from one publication, an identifier suffix is added. The naming of this identifier is based on the naming in the original database files or the proxy type (e.g. $\delta^{18}O$, Sr/Ca, etc.).

Most treering records were taken from the dataset used by Mann et al. (2008), which is a reduced set derived from the International treering Data Bank (ITRDB, version 5.03; www.ncdc.noaa.gov/paleo/treering.html). The naming for these series has not changed from the original (an abbreviated location followed by a core number). The treering series were subject to the following selection criteria (Mann et al., 2008):

(i) series must cover at least the interval 1750 to 1970, (ii) correlation between individual cores for a given site must be 0.50 for this period, (iii) there must be at least eight samples during the screened period 1800–1960 and for every year used. Series that were redundant with other compilations [used in the Mann et al. (2008) study] were not included. Four other series were not included because of site- specific problems [...]. Of the remaining series, [some] had to be replaced because of format errors in the chronology file on the ITRDB [...], or because sample depth data were missing from the chronology file. [...] When sample depth data were absent, the raw ring-width data from ITRDB were used to recalculate the chronology using program ARSTAN (Version 6.05P), with the following settings: a) a single detrending fitting a cubic spline of 50% variance reduction function at 66.6% the length of each sample, no stabilization

18

of variance or autoregressive modeling, indices computed as ratio, that is measurement

595   divided by curve, and chronology calculated as biweight robust mean estimate.

The Tierney et al. (2015) coral dataset is a comprehensive compilation of coral data covering the last ~400 years. Most of the records in this database were used in this study as temperature proxies, with the following exceptions:

  – DeLong et al. (2012, 2013, 2014) were replaced by the coral-derived SST series as presented
600   in original publications

  – Zinke et al. (2004); Kuhnert et al. (1999) were replaced by the coral-derived SST series as presented in Zinke et al. (2014)

  – Goodkin et al. (2008) $\delta^{18}O$ and Sr/Ca were replaced by the coral-derived SST series as presented in the original publication

605   – Pfeiffer et al. (2004) was excluded as the original publication shows that advection-induced SSS changes dominates over temperature in the coral $\delta^{18}O$ on interannual timescales

  – Swart et al. (1996b) was excluded as the original authors find no interannual $\delta^{18}O$-temperature relationship

  – Swart et al. (1996a) was excluded as the original publication shows SSS dominates the inter-
610   annual $\delta^{18}O$ signal and the $\delta^{18}O$-precipitation relationship is unstable

  – For Abram et al. (2008); Cole et al. (1993); Nakamura et al. (2009), the coral $\delta^{18}O$ signal is not clearly dominated by temperature but is a combination of T and P

  – For Cobb et al. (2003); Felis et al. (2000, 2009); Gorman et al. (2012); Linsley et al. (2006); Urban et al. (2000); Zinke et al. (2008), the coral $\delta^{18}O$ signal is not clearly dominated by
615   temperature but is a combination of T and SSS

  – Linsley et al. (1994) is interpreted as a precipitation record as the original study shows the $\delta^{18}O$ signal is 80% precipitation influence

  – Felis et al. (2009) Sr/Ca and $\delta^{18}O$, Kuhnert et al. (2005) Sr/Ca, Quinn et al. (1996), Quinn et al. (2006) Sr/Ca, Kilbourne et al. (2008) Sr/Ca and Druffel and Griffin (1999) $\delta^{18}O$
620   were excluded as their correlations with SST reported in Tierney et al. (2015) were of opposite sign to what is expected (i.e. positive when the physical processes should lead to a negative correlation)

Additional treering and coral records were retrieved from the NOAA Paleoclimatology Database (http://www.ncdc.noaa.gov/data-access/paleoclimatology-data/datasets) and were used as presented
625   there. Where available, temperature or precipitation reconstructions were used (i.e. where the raw

19

proxy series has already been converted). This was done to minimise biases due to nonlinearities in the raw proxy data which are accounted for in the conversion process. In some cases, two precipitation series were available for different seasons; these were summed (or averaged, depending on the type of data) to get a better approximate of an annual signal. While this may not be entirely accurate, annual signals are more desirable for the purpose of this study. Moreover, summing the records as opposed to treating them as individual records makes very little difference due to the nature of the method (weighting and summing the series). For corals, spliced records were used where available to maximise their length.

Proxy records with dating errors > 60 years were excluded from the analysis. The dating error was taken from the original publications where it was reported; otherwise it was derived from the age model results in the raw data files. In the latter case, the maximum error reported for the past 2000 years was used; larger errors further back in time were thus not taken into account as they are irrelevant for this study.

Appendix B: Detailed methods

The method developed in this study was used to create separate temperature and precipitation-based reconstructions of ENSO-like climate change made from weighted temperature and precipitation proxy records respectively. The weights were based on Empirical Orthogonal Function (EOF) patterns derived from general circulation models (GCMs) and the Twentieth Century Reanalysis Project Version 2c (20CRv2c). First, an ensemble of 'optimal' proxy networks is created using a GCM-based cross-validated 'add-one-in' approach. These networks are then applied to real proxy data to create a separate precipitation and temperature reconstruction of ENSO-like climate change over the past two millennia. Each step is described in more detail below.

B1 Empirical Orthogonal Function analysis

Empirical Orthogonal Function (EOF) analysis decomposes a spatiotemporal dataset into stationary time-varying coefficients. For a dataset of spatial resolution $x \times y$ and n time steps, it produces n maps (EOFs) of $x \times y$. The first map (EOF1) captures the largest fraction of variance of the original data. Each subsequent map maximises the amount of remaining variance captured, whilst being completely uncorrelated (orthogonal) to all preceding maps. Every EOF map is accompanied by a principal component (PC) timeseries of length n, which describes how the magnitude and sign of the EOF pattern varies over n. The first few EOFs can usually be attributed to physical dynamical phenomena such as seasonality or ENSO. By only retaining the leading EOFs, a dataset can be 'cleaned' of the (assumedly) random noise captured by the lower-order EOFs.

EOF analysis was applied to the 20CRv2c annual mean surface temperature and precipitation rate datasets to extract ENSO-like temperature and precipitation patterns respectively. The EOF patterns

660 were derived from annual data because while this study does not attempt to reconstruct interannual variability, it is concerned with climate changes that exhibit the classic ENSO-like spatial pattern. The EOFs were selected on the basis of their ability to capture the temporal evolution ENSO, measured by comparing the PC timeseries to three ENSO indices: MEI.ext (Wolter and Timlin, 2011), NINO3.4 and SOI (both available from http://www.cpc.ncep.noaa.gov/data/indices/). In both tem-

665 perature and precipitation, EOF2 displayed the signature ENSO pattern and had the highest correlation with the ENSO indices (precipitation $R^2 > 0.62$, temperature $R^2 > 0.66$), and was thus selected as a basis for weighting the proxies. The precipitation and temperature EOF2 explain 11.57% and 9.75% of variance, respectively. These EOFs were used for the final reconstructions of ENSO-like climate change.

670 **B2   GCM data**

For the creation of the network ensemble, GCM data was employed. The objective of the 'add-one-in' method is to create networks which accurately reconstruct the long-term (30-year averaged) ENSO signal. 20CRv2c covers less than 200 years, which is too short for meaningful evaluation of low-frequency change, particularly if the dataset is to be partitioned into calibration and validation

675 sets. GCMs, meanwhile, offer much longer datasets. Although they cannot simulate the real temporal climate change and variability of the past 1000 years, they are still useful for the building of proxy network ensembles, which asks only that they simulate realistic modes of spatiotemporal variability (i.e. EOF patterns). For the pseudoproxy experiment, the past1000 runs from two different GCMs were used for calibration (GCM_{cal}) and validation (GCM_{val}).

680   The following six GCMs (followed by their climate modelling groups in brackets) were considered as they have past1000 runs available:

- CCSM4 (National Center for Atmospheric Research)

- GISS-E2-R (NASA Goddard Institute for Space Studies)

- MPI-ESM-P (Max-Planck-Institut für Meteorologie (Max Planck Institute for Meteorology))

685   - IPSL-CM5A-LR (Institutenstitut Pierre-Simon Laplace)

- BCC-CSM1-1 (Beijing Climate Center, China Meteorological Administration)

- MIROC-ESM (Atmosphere and Ocean Research Institute (The University of Tokyo), National Institute for Environmental Studies, and Japan Agency for Marine-Earth Science and Technology)

690 All model datasets were regridded to 2°×3°.

    Each GCM produces a different ENSO-like EOF pattern, with varying biases (Bellenger et al., 2014; Collins, 2005); there is further variation among the different model runs. For this study, the

21

most 'accurate' GCM past1000 runs were selected, in the sense that their EOF values at proxy locations were most similar to the corresponding 20CRv2c values, which is the most realistic EOF pattern of modern-day ENSO available here. The real modern ENSO pattern will be different again, as will the real ENSO pattern of the past 1–2 millennia. By calibrating and validating the networks on datasets with slightly varying realisations of this ENSO pattern, the sensitivity of the networks to these variations is tested. EOF analysis was performed on the piControl and past1000 runs of the six GCMs, for precipitation and temperature separately. For each analysis, the first three EOFs were retained for comparison to the 20CRv2c ENSO-like EOF. The GCM EOF values of grid boxes with proxies were compared to the corresponding 20CRv2c grid boxes via Pearson rank correlation. The two GCMs with the highest correlations with 20CRv2c across the two runs were chosen as GCM_{cal} and GCM_{val} for precipitation and temperature separately. As a result, CCSM4 ($R \geq 0.79$ in piControl and past1000) and GISS-E2-R ($R \geq 0.75$) were chosen as GCM_{cal} and GCM_{val} for precipitation; ISPL-CM5A-LR ($R \geq 0.46$) and BCC-CSM1-1 ($R \geq 0.44$) were chosen as GCM_{cal} and GCM_{val} for temperature.

B3 Pseudoproxies

Since there is no straightforward way of assessing the quality or relevance of a proxy beyond the selection criteria already discussed, a pseudoproxy approach can aid in making a more objective and refined decision on how to optimise the use of available proxy data (Smerdon, 2012). Since for pseudoproxies the 'real world' is known (in this case the GCM derived EOFs and PCs), it is possible to quantify the skill of the reconstruction. While a 'blanket' approach (in which every available record is used) may sound attractive, it increases the risk that some covarying, non-white noise in a subset of the proxies skews the resulting reconstruction. This is, for example, pertinent in North America where there is high clustering of treering records. Testing showed that when all records were added to the reconstruction, a regional trend obscured the ENSO-like signal (not shown). The only case in which it is certain that using all available proxies is preferred, is when each gridbox contains a (non-climatic) noise-free proxy such that the network gives complete spatial and temporal coverage.

Pseudoproxies are model or instrumental data series that are degraded by applying transformations and/or adding noise to simulate the behaviour of a real proxy (Mann, 2002). Proxy system models (Evans et al., 2013; Dee et al., 2015) attempt to characterise the mechanistic and forward processes connecting the response of a proxy archive to an environmental signal and the subsequent observation of this response; this includes accounting for nonlinearities, multivariate responses, and measurement limitations. Many PSMs require an isotope-enabled GCM or other data not available in the original sources of the proxy data collected for this study, but the VSLite model is an easily implemented PSM for simulating treering widths (TRW) which needs minimal input (Tolwinski-Ward et al., 2011; Breitenmoser et al., 2014; Evans et al., 2014). Using the R package *VSLiteR* available from GitHub (https://github.com/suztolwinskiward/VSLiteR), GCM precipitation and temperature

data were combined to create pseudo-TRW datasets, with which TRW proxies were represented in
the pseudoproxy experiment here. The rest of the proxies were represented by the GCM raw temperature or precipitation series.

These precipitation, temperature and TRW series (taken from the real proxy locations) were firstly degraded by adding white Gaussian noise. Information on true signal-to-noise ratios (SNR) of the various proxies is sparse in the literature. However, where data was available on the relationship between the proxy and the target climate variable in the form of R-values, SNR can be calculated via the following equation (Smerdon, 2012):

$$SNR = \frac{R}{\sqrt{1 - R^2}} \tag{B1}$$

Several original publications on individual publications provide such information(see Tables 1 and 2), and Tierney et al. (2015) have conducted a systematic comparison of most coral records included here against the Hadley Centre Global Sea Ice and Sea Surface Temperature (HadISST) 1900-1990 dataset. Where no concrete information was available, a value of SNR=0.4 was prescribed. While this has been shown to be a realistic average (Smerdon, 2012), comparison with the calculated SNRs in this study suggests it is in fact a relatively conservative value.

After the addition of noise, the pseudoproxies were degraded further to reflect the length, timespan and resolution of the real proxies. Real proxies' temporal resolution between 0-1000 yrBP was applied; this period was chosen as it is the focus of this stuδy. The resolution was recreated by assuming that each data point represents an average of the previous unsampled years; for example in a proxy with a 10-year resolution, data point n was recreated by taking the average over points $(n-9) : n$.

B4   Calibration: network creation

After screening proxy records, selecting GCMs and creating pseudoproxies, a pseudoproxy experiment was conducted to create an 'optimal network' ensemble. The calibration stage builds proxy networks in a stepwise manner by incrementally adding the proxy that maximally improves the quality of the network reconstruction. All proxies were first subjected to inverse transform sampling (ITS) using the MATLAB script (translated to R) available at https://github.com/CommonClimate/commonclimate/blob/master/gaussianize.m. ITS converts the distribution of a timeseries to a standard normal distribution, thus reducing the bias introduced by nonlinearities inherent to many proxy records (Emile-Geay and Tingley, 2016). Lastly, the pseudoproxies were averaged to 30 years (using a simple average) to prevent high-resolution records from dominating the signal. This averaging period was chosen as our focus is on long-term ENSO state rather than inter-annual variability, and reflects the resolution of many individual low-frequency proxy reconstructions (cf Yan et al., 2011a, b; Anderson, 2012; Rodysill et al., 2012; Makou et al., 2010). Then at each stage (for each interim network), the pseudoproxies in the network (derived from GCM_{cal} past1000) were first normalised

23

to a common period $(a : b)$ where all proxies data via the equation:

$$Pn_t = \frac{P_t - \mu_{a:b}}{\sigma_{a:b}} \tag{B2}$$

where Pn_t is the normalised proxy value at time t, P_t is the original value at time t, $\mu_{a:b}$ is the mean value of proxy P between common period $a : b$, and $\sigma_{a:b}$ is the corresponding standard deviation. The length of $a : b$ was ensured to be at least 100 years to reduce the influence of noise on μ and σ. In some cases, this requirement led to the rejection of one or more proxies as their length or position in time were not compatible with the other records. This process of normalisation is similar to the method used in Wilson et al. (2010). Proxies that fall in the same grid box were averaged after normalisation. This prevents overrepresentation of those locations, and improves their SNR by cancelling out some of the stochastic noise and amplifying their signal (Wang et al., 2014).

Each normalised pseudoproxy Pn at location $[x, y]$ was multiplied by a scaled version of the EOF value at location $[x, y]$. The scaling was such that at each timestep the absolute sum of the weights was 1, which accounts for the fact that the number of locations with proxy data varies over the reconstructed period (especially the beginning and end). The weight of a given proxy location i can thus be considered an indication of the relative sensitivity of a location to ENSO which changes depending on the number of proxies n available at each timestep t and their associated EOF values W:

$$Wn_{it} = \frac{W_{it}}{\sum_{i=1}^{n} |W_{it}|} \tag{B3}$$

Finally, the n weighted proxy series Pw were summed to create a single reconstruction series $ENSO_r$:

$$Pw_t = P_t \times Wn_{Pt} \tag{B4}$$

$$ENSO_r = \sum_{i=1}^{n} Pw_i \tag{B5}$$

This is essentially a 'sparse' reconstruction of the PC, which is the dot product of the full raw dataset and EOF. The quality of a network was assessed by comparing $ENSO_r$ with the PC using the Pearson rank correlation R.

The entire calibration process was repeated 1000 times, each time using pseudoproxies with newly generated noise iterations, resulting in 1000 proxy networks.

B5 Validation: network evaluation

The validation stage tests the robustness of the networks using independent data. A 1000 pseudo-proxy versions were created of each calibration network using GCM_{val} pseudoproxies, and tested for their ability to reconstruct the target (the PC created using the GCM_{cal} EOF and the GCM_{val} past1000 dataset) by calculating R. There are several measures of quality for validation statistics, the most common of which are the coefficient of determination R^2, the reduction of error (RE)

and the coefficient of efficiency (CE; Cook et al., 1994). Discussions on the relative merits and pitfalls of these measures can be found in the literature (cf Cook et al., 1995; Emile-Geay et al., 2013a). Although CE is generally regarded as the appropriate indicator for low-frequency reconstructions (Bürger, 2007; Emile-Geay et al., 2013a), the nature of the method described here reduces its effectiveness as a measure of quality. The past1000 and piControl runs have little (or no) external forcing driving the simulation, hence they have very little low-frequency variability or trends. Moreover, the data is z-normalised at various stages, removing any differences in means. As the CE effectively tracks changes in the mean, this removal of the mean renders CE sensitive to spurious results. The diagnostic R was instead chosen as tests showed that it was more effective at picking high-quality reconstructions than CE and $RMSE$, though generally a high R value did correspond to high CE and low $RMSE$ (not shown). R is essentially equivalent to using R^2, but retains the ability to distinguish between positive and negative correlations.

The R-values from the 1000×1000 validation reconstructions (R_{val}) were then compared to critical values R_{crit} calculated for each network. Again, 1000 reconstructions were made for each network, but using GCM$_{val}$ piControl data instead of past1000. The piControl run contains no external forcing and so is essentially noise, but retains the inherent climatological spatial correlations. From these reconstructions, R_{crit} for each network was determined by taking the 95th percentile of the R-values of the corresponding 1000 reconstructions. Where $R_{val} > R_{crit}$, the network was retained; where $R_{val} < R_{crit}$, the network was deemed unfit and was discarded. Networks sensitive to the choice of dataset are thus weeded out.

The combination of using pseudoproxies, the add-one-in approach and R_{crit} simultaneously accounts for proxy temporal resolution, spatial distribution and temporal coverage (i.e. proxy start and end dates), and gives an estimate of the uncertainty due to proxy noise. However, an important assumption is that the *signal* in all proxies is solely temperature or precipitation, and it is thus still a 'best case' estimate.

B6   Proxy ENSO ensemble

The 'optimal' networks that passed the R_{crit} test were used to create an ensemble of real proxy reconstructions of ENSO-like climate change. The remaining networks may not all be unique, further reducing the effective number of networks. Presumably, networks that occur multiple times are more effective proxy combinations; retaining the duplicates accordingly upweights these networks in the final reconstruction. Error estimates for the reconstructions were made using the 1000×1000 $RMSE$ values calculated at the validation stage. This was translated into ensemble member uncertainty limits by adding and subtracting the 1000 error series from the reconstruction timeseries (to get the maximum and minimum error limits respectively) and taking the 5-95th percentile over their full range. This error estimation explicitly takes into account the impact of network choice as well as random error affecting the proxies.

Once proxy reconstructions and associated uncertainty estimates were calculated for all ensemble members, they were renormalised to 100-650 yrBP to make the trends and amplitudes comparable, within and between temperature and precipitation. The period 100-650 yrBP was chosen because it was common to all reconstruction timeseries and only covers one of the two periods of interest (the LIA). Although calibration to the instrumental period would potentially allow us to quantify the absolute amplitude, this was not done for two reasons. Firstly, the proxy data coverage during the instrumental period and the preceding century was relatively low, reducing the confidence in the reconstruction during that period; calibrating to this period would thus increase the uncertainty on the rest of the reconstruction. Secondly, any calibration to the instrumental data is necessarily biased towards high-frequency trends (Mann et al., 2008). Within a 30-year averaged series, the number of comparison points with the instrumental period is extremely low. The final proxy reconstruction was calculated as the ensemble mean. The corresponding error estimate is a combination of the reconstruction ensemble range and the error ranges for individual ensemble members.

References

Abram, N. J., Gagan, M. K., Cole, J. E., Hantoro, W. S., and Mudelsee, M.: Recent intensification of tropical climate variability in the Indian Ocean, Nat. Geosci., 1, 849–853, doi:10.1038/ngeo357, 2008.

865 Abram, N. J., McGregor, H. V., Gagan, M. K., Hantoro, W. S., and Suwargadi, B. W.: Oscillations in the southern extent of the Indo-Pacific Warm Pool during the mid-Holocene, Quat. Sci. Rev., 28, 2794–2803, doi:10.1016/j.quascirev.2009.07.006, 2009.

Alibert, C. and Kinsley, L.: A 170-year Sr/Ca and Ba/Ca coral record from the western Pacific warm pool: 2. A window into variability of the New Ireland Coastal Undercurrent, J. Geophys. Res. Ocean., 113, 1–10,

870 doi:10.1029/2007JC004263, 2008.

Anchukaitis, K. J. and Evans, M. N.: Tropical cloud forest climate variability and the demise of the Monteverde golden toad., Proc. Natl. Acad. Sci. U. S. A., 107, 5036–5040, doi:10.1073/pnas.0908572107, 2010.

Anchukaitis, K. J., Evans, M. N., Kaplan, A., Vaganov, E. A., Hughes, M. K., Grissino-Mayer, H. D., and Cane, M. A.: Forward modeling of regional scale tree-ring patterns in the southeastern United States and the recent

875 influence of summer drought, Geophys. Res. Lett., 33, 2–5, doi:10.1029/2005GL025050, 2006.

Anderson, L.: Holocene record of precipitation seasonality from lake calcite δ^{18}O in the central Rocky Mountains, United States, Geology, 39, 211–214, doi:10.1130/G31575.1, 2011.

Anderson, L.: Rocky Mountain hydroclimate: Holocene variability and the role of insolation, ENSO, and the North American Monsoon, Glob. Planet. Change, 92-93, 198–208, doi:10.1016/j.gloplacha.2012.05.012,

880 2012.

Apastaégui, J., Cruz, F. W., Sifeddine, A., Vuille, M., Espinoza, J. C., Guyot, J. L., Khodri, M., Strikis, N., Santos, R. V., Cheng, H., Edwards, L., Carvalho, E., and Santini, W.: Hydroclimate variability of the northwestern Amazon Basin near the Andean foothills of Peru related to the South American Monsoon System during the last 1600 years, Clim. Past, 10, 1967–1981, doi:10.5194/cp-10-1967-2014, 2014.

885 Asami, R.: Interannual and decadal variability of the western Pacific sea surface condition for the years 1787–2000: Reconstruction based on stable isotope record from a Guam coral, J. Geophys. Res., 110, C05 018, doi:10.1029/2004JC002555, 2005.

Ashok, K., Behera, S. K., Rao, S. A., Weng, H., and Yamagata, T.: El Niño Modoki and its possible teleconnection, J. Geophys. Res. Ocean., 112, 1–27, doi:10.1029/2006JC003798, 2007.

890 Asmerom, Y., Polyak, V., Burns, S. J., and Rassmussen, J.: Solar forcing of Holocene climate: New insights from a speleothem record, southwestern United States, Geology, 35, 1–4, doi:10.1130/G22865A.1, 2007.

Badjeck, M.-C., Allison, E. H., Halls, A. S., and Dulvy, N. K.: Impacts of climate variability and change on fishery-based livelihoods, Mar. Policy, 34, 375–383, doi:10.1016/j.marpol.2009.08.007, 2010.

Bagnato, S., Linsley, B. K., Howe, S. S., Wellington, G. M., and Salinger, J.: Coral oxygen isotope records

895 of interdecadal climate variations in the South Pacific Convergence Zone region, Geochemistry, Geophys. Geosystems, 6, 1–8, doi:10.1029/2004GC000879, 2005.

Baker, P. A., Fritz, S. C., Burns, S. J., Ekdahl, E., and Rigsby, C. A.: The Nature and Origin of Decadal to Millennial Scale Climate Variability in the Southern Tropics of South America: The Holocene Record of Lago Umayo, Peru, in: Past Clim. Var. South Am. Surround. Reg. From Last Glacial Maximum to Holocene,

900 edited by Vimeux, F., Sylvestre, F., and Khodri, M., chap. 13, pp. 301–322, Springer Netherlands, Dordrecht, 14 edn., doi:10.1007/978-90-481-2672-9_13, 2009.

Barron, J. A.: High-resolution climatic evolution of coastal northern California during the past 16,000 years, Paleoceanography, 18, doi:10.1029/2002PA000768, 1020, 2003.

Barron, J. A. and Anderson, L.: Enhanced Late Holocene ENSO/PDO expression along the margins of the eastern North Pacific, Quat. Int., 235, 3–12, doi:10.1016/j.quaint.2010.02.026, 2011.

Bellenger, H., Guilyardi, E., Leloup, J., Lengaigne, M., and Vialard, J.: ENSO representation in climate models: From CMIP3 to CMIP5, Clim. Dyn., 42, 1999–2018, doi:10.1007/s00382-013-1783-z, 2014.

Berke, M. A., Johnson, T. C., Werne, J. P., Schouten, S., and Sinninghe Damsté, J. S.: A mid-Holocene thermal maximum at the end of the African Humid Period, Earth Planet. Sci. Lett., 351-352, 95–104, doi:10.1016/j.epsl.2012.07.008, 2012.

Bird, B. W., Abbott, M. B., Rodbell, D. T., and Vuille, M.: Holocene tropical South American hydroclimate revealed from a decadally resolved lake sediment $\delta^{18}O$ record, Earth Planet. Sci. Lett., 310, 192–202, doi:10.1016/j.epsl.2011.08.040, 2011.

Black, D. E., Abahazi, M. A., Thunell, R. C., Kaplan, A., Tappa, E. J., and Peterson, L. C.: An 8-century tropical Atlantic SST record from the Cariaco Basin: Baseline variability, twentieth-century warming, and Atlantic hurricane frequency, Paleoceanography, 22, 1–10, doi:10.1029/2007PA001427, 2007.

Boiseau, M., Ghil, M., and Juillet-Leclerc, A.: Climatic trends and interdecadal variability from South-Central Pacific coral records, Geophys. Res. Lett., 26, 2881–2884, 1999.

Bonnefille, R. and Chalié, F.: Pollen-inferred precipitation time-series from equatorial mountains, Africa, the last 40 kyr BP, Glob. Planet. Change, 26, 25–50, doi:10.1016/S0921-8181(00)00032-1, 2000.

Braconnot, P., Harrison, S. P., Otto-Bliesner, B. L., Abe-Ouchi, A., Jungclaus, J. H., and Peterschmitt, J.-Y.: The Paleoclimate Modeling Intercomparison Project contribution to CMIP5, CLIVAR Exch. Newsl., 16, 15–19, 2011.

Braconnot, P., Harrison, S. P., Kageyama, M., Bartlein, P. J., Masson-Delmotte, V., Abe-Ouchi, A., Otto-Bliesner, B., and Zhao, Y.: Evaluation of climate models using palaeoclimatic data, Nat. Clim. Chang., 2, 417–424, doi:10.1038/nclimate1456, 2012.

Braganza, K., Gergis, J. L., Power, S. B., Risbey, J. S., and Fowler, A. M.: A multiproxy index of the El Niño-Southern Oscillation, A.D. 1525-1982, J. Geophys. Res. Atmos., 114, 1–17, doi:10.1029/2008JD010896, 2009.

Breitenmoser, P., Brönnimann, S., and Frank, D.: Forward modelling of tree-ring width and comparison with a global network of tree-ring chronologies, Clim. Past, 10, 437–449, doi:10.5194/cp-10-437-2014, 2014.

Brook, G., Sheen, S.-W., Rafter, M., Railsback, L. B., and Lundberg, J.: A high-resolution proxy record of rain-fall and ENSO since AD 1550 from layering in stalagmites from Anjohibe Cave, Madagascar, The Holocene, 9, 695–705, doi:10.1191/095968399677907790, 1999.

Buckley, B. M., Anchukaitis, K. J., Penny, D., Fletcher, R., Cook, E. R., Sano, M., Nam, L. C., Wichienkeeo, A., Minh, T. T., and Hong, T. M.: Climate as a contributing factor in the demise of Angkor, Cambodia., Proc. Natl. Acad. Sci. U. S. A., 107, 6748–6752, doi:10.1073/pnas.0910827107, 2010.

Bürger, G.: On the verification of climate reconstructions, Clim. Past, 3, 397–409, doi:10.5194/cpd-3-249-2007, 2007.

940 Cai, W., Santoso, A., Wang, G., Yeh, S.-w., An, S.-i., Cobb, K. M., Collins, M., Guilyardi, E., Jin, F.-f., Kug, J.-s., Lengaigne, M., and McPhaden, M. J.: ENSO and greenhouse warming, Nat. Publ. Gr., 5, 849–859, doi:10.1038/nclimate2743, 2015a.

Cai, W., Wang, G., Santoso, A., McPhaden, M. J., Wu, L., Jin, F.-F., Timmermann, A., Collins, M., Vecchi, G., Lengaigne, M., England, M. H., Dommenget, D., Takahashi, K., and Guilyardi, E.: Increased frequency of ex-
945 treme La Niña events under greenhouse warming, Nat. Clim. Chang., 5, 132–137, doi:10.1038/nclimate2492, 2015b.

Cane, M. A.: The evolution of El Niño, past and future, Earth Planet. Sci. Lett., 230, 227–240, doi:10.1016/j.epsl.2004.12.003, 2005.

Carré, M., Bentaleb, I., Fontugne, M., and Lavallée, D.: Strong El Niño events during the early Holocene: sta-
950 ble isotope evidence from Peruvian sea shells, The Holocene, 15, 42–47, doi:10.1191/0959683605hl782rp, 2005.

Charles, C. D.: Interaction Between the ENSO and the Asian Monsoon in a Coral Record of Tropical Climate, Science, 227, 925–928, doi:10.1126/science.277.5328.925, 1997.

Charles, C. D., Cobb, K. M., Moore, M. D., and Fairbanks, R. G.: Monsoon-tropical ocean interaction in
955 a network of coral records spanning the 20th century, Mar. Geol., 201, 207–222, doi:10.1016/S0025-3227(03)00217-2, 2003.

Chen, J., Chen, F., Zhang, E., Brooks, S. J., Zhou, A., and Zhang, J.: A 1000-year chironomid-based salinity reconstruction from varved sediments of Sugan Lake, Qaidam Basin, arid Northwest China, and its palaeo-climatic significance, Chinese Sci. Bull., 54, 3749–3759, doi:10.1007/s11434-009-0201-8, 2009.

960 Christie, D. A., Boninsegna, J. A., Cleaveland, M. K., Lara, A., Le Quesne, C., Morales, M. S., Mudelsee, M., Stahle, D. W., and Villalba, R.: Aridity changes in the Temperate-Mediterranean transition of the Andes since AD 1346 reconstructed from tree-rings, Clim. Dyn., 36, 1505–1521, doi:10.1007/s00382-009-0723-4, 2011.

Cleaveland, M. K., Stahle, D. W., Therrell, M. D., Villanueva-Diaz, J., and Burns, B. T.: Tree-ring recon-structed winter precipitation and tropical teleconnections in Durango, Mexico, Clim. Change, 59, 369–388,
965 doi:10.1023/A:1024835630188, 2003.

Clement, A. C., Cane, M. A., and Seager, R.: An orbitally driven tropical source for abrupt climate change, J. Clim., 14, 2369–2375, doi:10.1175/1520-0442(2001)014<2369:AODTSF>2.0.CO;2, 2001.

Coats, S., Smerdon, J. E., Cook, B. I., and Seager, R.: Stationarity of the tropical pacific teleconnection to North America in CMIP5/PMIP3 model simulations, Geophys. Res. Lett., 40, 4927–4932, doi:10.1002/grl.50938,
970 2013.

Cobb, K. M., Charles, C. D., Cheng, H., and Edwards, R. L.: El Niño/Southern Oscillation and tropical Pacific climate during the last millennium., Nature, 424, 271–276, doi:10.1038/nature01779, 2003.

Cole, J. E.: Tropical Pacific forcing of decadal SST variability in the western Indian Ocean over the past two centuries, Science, 287, 617–619, doi:10.1126/science.287.5453.617, 2000.

975 Cole, J. E., Fairbanks, R. G., and Shen, G. T.: Recent variability in the Southern Oscillation: isotopic results from a tarawa atoll coral., Science, 260, 1790–1793, doi:10.1126/science.260.5115.1790, 1993.

Collins, M.: El Niño- or La Niña-like climate change?, Clim. Dyn., 24, 89–104, doi:10.1007/s00382-004-0478-x, 2005.

Comboul, M., Emile-geay, J., Evans, M. N., Mirnateghi, N., Cobb, K. M., and Thompson, D. M.: A probabilistic model of chronological errors in layer-counted climate proxies: Applications to annually banded coral archives, Clim. Past, 10, 825–841, doi:10.5194/cp-10-825-2014, 2014.

Comboul, M., Emile-geay, J., Hakim, G. J., and Evans, M. N.: Paleoclimate Sampling as a Sensor Placement Problem, J. Clim., 28, 7717–7740, 2015.

Compo, G. P., Whitaker, J. S., Sardeshmukh, P. D., Matsui, N., Allan, R. J., Yin, X., Gleason, B. E., Vose, R. S., Rutledge, G., Bessemoulin, P., Bronnimann, S., Brunet, M., Crouthamel, R. I., Grant, A. N., Groisman, P. Y., Jones, P. D., Kruk, M. C., Kruger, A. C., Marshall, G. J., Maugeri, M., Mok, H. Y., Nordli, O., Ross, T. F., Trigo, R. M., Wang, X. L., Woodruff, S. D., and Worley, S. J.: The Twentieth Century Reanalysis Project, Q. J. R. Meteorol. Soc., 137, 1–28, doi:10.1002/qj.776, 2011.

Conroy, J., Overpeck, J. T., and Cole, J. E.: El Niño-Southern Oscillation and changes in the zonal gradient of tropical Pacific sea surface temperature over the last 1.2 ka, PAGES News, 18, 1–5, 2010.

Conroy, J. L., Overpeck, J. T., Cole, J. E., Shanahan, T. M., and Steinitz-Kannan, M.: Holocene changes in eastern tropical Pacific climate inferred from a Galápagos lake sediment record, Quat. Sci. Rev., 27, 1166–1180, doi:10.1016/j.quascirev.2008.02.015, 2008.

Conroy, J. L., Restrepo, A., Overpeck, J. T., Steinitz-Kannan, M., Cole, J. E., Bush, M. B., and Colinvaux, P. A.: Unprecedented recent warming of surface temperatures in the eastern tropical Pacific Ocean, Nat. Geosci., 2, 46–50, doi:10.1038/ngeo390, 2009.

Cook, E. R., Briffa, K. R., and Jones, P. D.: Spatial regression methods in dendroclimatology: A review and comparison of two techniques, Int. J. Climatol., 14, 379–402, doi:10.1002/joc.3370140404, 1994.

Cook, E. R., Briffa, K. R., Meko, D. M., Graybill, D. A., and Funkhouser, G.: The 'segment length curse' in long tree-ring chronology development for palaeoclimatic studies, The Holocene, 5, 229–237, 1995.

Cook, E. R., Buckley, B. M., D'Arrigo, R. D., and Peterson, M. J.: Warm-season temperatures since 1600 BC reconstructed from Tasmanian tree rings and their relationship to large-scale sea surface temperature anomalies, Clim. Dyn., 16, 79–91, doi:10.1007/s003820050006, 2000.

Corrège, T., Delcroix, T., Récy, J., Beck, W., Cabioch, G., and Le Cornec, F.: Evidence for stronger El Niño-Southern Oscillation (ENSO) events in a mid-Holocene massive coral, Paleoceanography, 15, 465–470, 2000.

Crausbay, S. D., Russell, J. M., and Schnurrenberger, D. W.: A ca. 800-year lithologic record of drought from sub-annually laminated lake sediment, East Java, J. Paleolimnol., 35, 641–659, doi:10.1007/s10933-005-4440-7, 2006.

Cronin, T. M., Dwyer, G. S., Kamiya, T., Schwede, S., and Willard, D. A.: Medieval Warm Period, Little Ice Age and 20th century temperature variability from Chesapeake Bay, Glob. Planet. Change, 36, 17–29, doi:10.1016/S0921-8181(02)00161-3, 2003.

Cronin, T. M., Thunell, R., Dwyer, G. S., Saenger, C., Mann, M. E., Vann, C., and Seal, I. R.: Multiproxy evidence of Holocene climate variability from estuarine sediments, eastern North America, Paleoceanography, 20, doi:10.1029/2005PA001145, 2005.

Curtis, J. H., Hodelle, D. A., and Brenner, M.: Climate variability on the Yucatán Peninsula (Mexico) during the past 3500 years, and implications for Maya cultural evolution, Quat. Res., 46, 37–47, doi:10.1006/qres.1996.0042, 1996.

Damassa, T. D., Cole, J. E., Barnett, H. R., Ault, T. R., and McClanahan, T. R.: Enhanced multidecadal climate variability in the seventeenth century from coral isotope records in the western Indian Ocean, Paleoceanography, 21, PA2016, doi:10.1029/2005PA001217, 2006.

D'Arrigo, R. and Wilson, R.: On the Asian expression of the PDO, Int. J. Climatol., 26, 1607–1617, doi:10.1002/joc.1326, 2006.

Dee, S., Emile-Geay, J., Evans, M. N., Allam, A., Steig, E. J., and Thompson, D. M.: PRYSM: An open-source framework for PRoxY System Modeling, with applications to oxygen-isotope systems, J. Adv. Model. Earth Syst., 7, 1220–1247, doi:10.1002/ 2015MS000447, 2015.

DeLong, K. L., Quinn, T. M., Taylor, F. W., Lin, K., and Shen, C.-C.: Sea surface temperature variability in the southwest tropical Pacific since AD 1649, Nat. Clim. Chang., 2, 799–804, doi:10.1038/nclimate1583, 2012.

DeLong, K. L., Quinn, T. M., Taylor, F. W., Shen, C. C., and Lin, K.: Improving coral-base paleoclimate reconstructions by replicating 350years of coral Sr/Ca variations, Palaeogeogr. Palaeoclimatol. Palaeoecol., 373, 6–24, doi:10.1016/j.palaeo.2012.08.019, 2013.

DeLong, K. L., Flannery, J. A., Poore, R. Z., Quinn, T. M., Maupin, C. R., Lin, K., and Shen, C. C.: A reconstruction of sea surface temperature variability in the southeastern Gulf of Mexico from 1734 to 2008 C.E. using cross-dated Sr/Ca records from the coral Siderastrea siderea, Paleoceanography, 29, 403–422, doi:10.1002/2013PA002524, 2014.

Denniston, R. F., Villarini, G., Gonzales, A. N., Wyrwoll, K.-H., Polyak, V. J., Ummenhofer, C. C., Lachniet, M. S., Wanamaker, A. D., Humphreys, W. F., Woods, D., and Cugley, J.: Extreme rainfall activity in the Australian tropics reflects changes in the El Niño/Southern Oscillation over the last two millennia., Proc. Natl. Acad. Sci. U. S. A., 112, 4576–4581, doi:10.1073/pnas.1422270112, 2015.

Díaz, S. C., Therrell, M. D., Stahle, D. W., and Cleaveland, M. K.: Chihuahua (Mexico) winter-spring precipitation reconstructed from tree-rings, 1647-1992, Clim. Res., 22, 237–244, doi:10.3354/cr022237, 2002.

Druffel, E. R. M. and Griffin, S.: Variability of surface ocean radiocarbon and stable isotopes in the southwestern Pacific, J. Geophys. Res. Ocean., 104, 23 607–23 613, doi:10.1029/1999jc900212, 1999.

Dunbar, R. B., Wellington, G. M., Colgan, M. W., and Glynn, P. W.: Eastern Pacific sea surface temperature since 1600 A.D.: The $\delta^{18}O$ record of climate variability in Galápagos Corals, Paleoceanography, 9, 291–315, doi:10.1029/93PA03501, 1994.

Emile-Geay, J. and Tingley, M.: Inferring climate variability from nonlinear proxies. Application to paleo-ENSO studies., Clim. Past, 12, 31–50, doi:10.5194/cp-12-31-2016, 2016.

Emile-Geay, J., Cobb, K. M., Mann, M. E., and Wittenberg, A. T.: Estimating central equatorial pacific SST variability over the past millennium. Part I: Methodology and validation, J. Clim., 26, 2302–2328, doi:10.1175/JCLI-D-11-00510.1, 2013a.

Emile-Geay, J., Cobb, K. M., Mann, M. E., and Wittenberg, A. T.: Estimating central equatorial pacific SST variability over the past millennium. Part II: Reconstructions and Implications, J. Clim., 26, 2329–2352, doi:10.1175/JCLI-D-11-00511.1, 2013b.

Esper, J., Cook, E. R., and Schweingruber, F. H.: Low-frequency signals in long tree-ring chronologies for reconstructing past temperature variability., Science, 295, 2250–2253, doi:10.1126/science.1066208, 2002.

Evans, M. N., Kaplan, A., and Cane, M. A.: Optimal sites for coral-based reconstruction of global sea surface temperature, Paleoceanography, 13, 502–516, doi:10.1029/98PA02132, 1998.

31

Evans, M. N., Tolwinski-Ward, S. E., Thompson, D. M., and Anchukaitis, K. J.: Applications of proxy system modeling in high resolution paleoclimatology, Quat. Sci. Rev., 76, 16–28, 2013.

Evans, M. N., Smerdon, J. E., Kaplan, A., Tolwinski-Ward, S. E., and González-Rouco, J. F.: Climate field reconstruction uncertainty arising from multivariate and nonlinear properties of predictors, Geophys. Res. Lett., 41, 9127–9134, doi:10.1002/2014GL062063, 2014.

Faulstich, H. L., Woodhouse, C. A., and Griffin, D.: Reconstructed cool- and warm-season precipitation over the tribal lands of northeastern Arizona, Clim. Change, 118, 457–468, doi:10.1007/s10584-012-0626-y, 2013.

Felis, T., Pätzold, J., Loya, Y., Fine, M., Nawar, A. H., and Wefer, G.: A coral oxygen isotope record from the northern Red Sea documenting NAO, ENSO, and North Pacific teleconnections on Middle East climate variability since the year 1750, Paleoceanography, 15, 679–694, doi:10.1029/1999PA000477, 2000.

Felis, T., Suzuki, A., Kuhnert, H., Dima, M., Lohmann, G., and Kawahata, H.: Subtropical coral reveals abrupt early-twentieth-century freshening in the western North Pacific Ocean, Geology, 37, 527–530, doi:10.1130/G25581A.1, 2009.

Felis, T., Suzuki, A., Kuhnert, H., Rimbu, N., and Kawahata, H.: Pacific decadal oscillation documented in a coral record of North Pacific winter temperature since 1873, Geophys. Res. Lett., 37, 2000–2005, doi:10.1029/2010GL043572, 2010.

Gallant, A. J. E., Phipps, S. J., Karoly, D. J., Mullan, A. B., and Lorrey, A. M.: Nonstationary Australasian teleconnections and implications for paleoclimate reconstructions, J. Clim., 26, 8827–8849, doi:10.1175/JCLI-D-12-00338.1, 2013.

Gomez, B., Carter, L., Trustrum, N. A., Palmer, A. S., and Roberts, A. P.: El Niño-Southern Oscillation signal associated with middle Holocene climate change in intercorrelated terrestrial and marine sediment cores, North Island, New Zealand, Geology, 32, 653–656, doi:10.1130/G20720.1, 2004.

Goni, M. A., Thunell, R. C., Woodwort, M. P., and Müller-Karger, F. E.: Changes in wind-driven upwelling during the last three centuries: Interocean teleconnections, Geophys. Res. Lett., 33, 3–6, doi:10.1029/2006GL026415, 2006.

Goodkin, N. F., Hughen, K. A., Curry, W. B., Doney, S. C., and Ostermann, D. R.: Sea surface temperature and salinity variability at Bermuda during the end of the Little Ice Age, Paleoceanography, 23, 1–13, doi:10.1029/2007PA001532, 2008.

Gorman, M. K., Quinn, T. M., Taylor, F. W., Partin, J. W., Cabioch, G., Austin, J. A., Pelletier, B., Ballu, V., Maes, C., and Saustrup, S.: A coral-based reconstruction of sea surface salinity at Sabine Bank, Vanuatu from 1842 to 2007 CE, Paleoceanography, 27, 1–13, doi:10.1029/2012PA002302, 2012.

Graham, N. E., Hughes, M. K., Ammann, C. M., Cobb, K. M., Hoerling, M. P., Kennett, D. J., Kennett, J. P., Rein, B., Stott, L., Wigand, P. E., and Xu, T.: Tropical Pacific - Mid-latitude teleconnections in medieval times, Clim. Change, 83, 241–285, doi:10.1007/s10584-007-9239-2, 2007.

Griffin, D., Woodhouse, C. A., Meko, D. M., Stahle, D. W., Faulstich, H. L., Carrillo, C., Touchan, R., Castro, C. L., and Leavitt, S. W.: North American monsoon precipitation reconstructed from tree-ring latewood, Geophys. Res. Lett., 40, 954–958, doi:10.1002/grl.50184, 2013.

Guilderson, T. P. and Schrag, D. P.: Reliability of coral isotope records from the Western Pacific Warm Pool: A comparison using age-optimized records, Paleoceanography, 14, 457, doi:10.1029/1999PA900024, 1999.

Guilyardi, E., Wittenberg, A., Fedorov, A., Collins, M., Wang, C., Capotondi, A., van Oldenborgh, G. J., and Stockdale, T.: Understanding El Niño in ocean-atmosphere general circulation models: Progress and challenges, Bull. Am. Meteorol. Soc., 90, 325–340, doi:10.1175/2008BAMS2387.1, 2009.

Haug, G. H., Hughen, K. A., Sigman, D. M., Peterson, L. C., and Röhl, U.: Southward migration of the intertropical convergence zone through the Holocene., Science, 293, 1304–1308, doi:10.1126/science.1059725, 2001.

Heiss, G. A.: Coral reefs in the Red Sea: Growth, production and stable isotopes., GEOMAR Rep., 32, 1–141, 1994.

Hendy, E. J., Gagan, M. K., and Lough, J. M.: Chronological control of coral records using luminescent lines and evidence for non-stationary ENSO teleconnections in northeast Australia, The Holocene, 13, 187–199, doi:10.1191/0959683603hl606rp, 2003.

Hetzinger, S., Pfeiffer, M., Dullo, W. C., Garbe-Schönberg, D., and Halfar, J.: Rapid 20th century warming in the Caribbean and impact of remote forcing on climate in the northern tropical Atlantic as recorded in a Guadeloupe coral, Palaeogeogr. Palaeoclimatol. Palaeoecol., 296, 111–124, doi:10.1016/j.palaeo.2010.06.019, 2010.

Hjelle, B. and Glass, G. E.: Outbreak of hantavirus infection in the Four Corners region of the United States in the wake of the 1997-1998 El Niño-Southern Oscillation., J. Infect. Dis., 181, 1569–1573, doi:10.1086/315467, 2000.

Hodell, D. A., Curtis, J. H., and Brenner, M.: Possible role of climate in the collapse of Classic Maya civilization, Nature, 375, 391–394, doi:10.1038/375391a0, 1995.

Ivanochko, T. S., Ganeshram, R. S., Brummer, G. J. a., Ganssen, G., Jung, S. J. a., Moreton, S. G., and Kroon, D.: Variations in tropical convection as an amplifier of global climate change at the millennial scale, Earth Planet. Sci. Lett., 235, 302–314, doi:10.1016/j.epsl.2005.04.002, 2005.

Jones, P., Briffa, K., Osborn, T., Lough, J., van Ommen, T., Vinther, B., Luterbacher, J., Wahl, E., Zwiers, F., Mann, M., Schmidt, G., Ammann, C., Buckley, B., Cobb, K., Esper, J., Goosse, H., Graham, N., Jansen, E., Kiefer, T., Kull, C., Küttel, M., Mosley-Thompson, E., Overpeck, J., Riedwyl, N., Schulz, M., Tudhope, A., Villalba, R., Wanner, H., Wolff, E. W., Xoplaki, E., Kuttel, M., Mosley-Thompson, E., Overpeck, J., Riedwyl, N., Schulz, M., Tudhope, A., Villalba, R., Wanner, H., Wolff, E. W., and Xoplaki, E.: High-resolution palaeoclimatology of the last millennium: a review of current status and future prospects, The Holocene, 19, 3–49, doi:10.1177/0959683608098952, 2009.

Jones, P. D. and Mann, M. E.: Climate over past millennia, Rev. Geophys., 42, 1–42, doi:10.1029/2003RG000143, 2004.

Karamperidou, C., Di Nezio, P. N., Timmermann, A., Jin, F. F., and Cobb, K. M.: The response of ENSO flavors to mid-Holocene climate: Implications for proxy interpretation, Paleoceanography, pp. 527–547, doi:10.1002/2014PA002742, 2015.

Keigwin, L. D.: The Little Ice Age and Medieval Warm Period in the Sargasso Sea, Science, 274, 1504–1508, doi:10.1126/science.274.5292.1504, 1996.

Kellerhals, T., Brütsch, S., Sigl, M., Knüsel, S., Gäggeler, H. W., and Schwikowski, M.: Ammonium concentration in ice cores: A new proxy for regional temperature reconstruction?, J. Geophys. Res. Atmos., 115, 1–8, doi:10.1029/2009JD012603, 2010.

33

Kennett, D., Breitenbach, S., Aquino, V., Asmerom, Y., Awe, J., Baldini, J., Bartlein, P., Culleton, B., Ebert, C., Jazwa, C., Macri, M., Marwan, N., Polyak, V., Prufer, K., Ridley, H., Sodemann, H., Winterhalder, B., and Haug, G.: Development and disintegration of Maya political systems in response to climate change., Science, 788, 788–791, doi:10.1126/science.1226299, 2012.

Khider, D., Jackson, C. S., and Stott, L. D.: Assessing millennial-scale variability during the Holocene: A perspective from the western tropical Pacific, Paleoceanography, 29, 143–159, doi:10.1002/2013PA002534, 2014.

Kilbourne, K. H., Quinn, T. M., Webb, R., Guilderson, T., Nyberg, J., and Winter, A.: Paleoclimate proxy perspective on Caribbean climate since the year 1751: Evidence of cooler temperatures and multidecadal variability, Paleoceanography, 23, 1–14, doi:10.1029/2008PA001598, 2008.

Kim, S. T. and Yu, J. Y.: The two types of ENSO in CMIP5 models, Geophys. Res. Lett., 39, 1–6, doi:10.1029/2012GL052006, 2012.

Klein, S. a., Soden, B. J., and Lau, N. C.: Remote sea surface temperature variations during ENSO: Evidence for a tropical atmospheric bridge, J. Clim., 12, 917–932, doi:10.1175/1520-0442(1999)012<0917:RSSTVD>2.0.CO;2, 1999.

Kovats, R. S., Bouma, M. J., Hajat, S., Worrall, E., and Haines, A.: El Niño and health, Lancet, 362, 1481–1489, 2003.

Krusic, P. J., Cook, E. R., Dukpa, D., Putnam, A. E., Rupper, S., and Schaefer, J.: Six hundred thirty-eight years of summer temperature variability over the Bhutanese Himalaya, Geophys. Res. Lett., 42, 2988–2994, doi:10.1002/2015GL063566.Received, 2015.

Kuhnert, H., Pätzold, J., Hatcher, B., Wyrwoll, K. H., Eisenhauer, A., Collins, L. B., Zhu, Z. R., and Wefer, G.: A 200-year coral stable oxygen isotope record from a high-latitude reef off Western Australia, Coral Reefs, 18, 1–12, doi:10.1007/s003380050147, 1999.

Kuhnert, H., Pätzold, J., Wyrwoll, K. H., and Wefer, G.: Monitoring climate variability over the past 116 years in coral oxygen isotopes from Ningaloo Reef, Western Australia, Int. J. Earth Sci., 88, 725–732, doi:10.1007/s005310050300, 2000.

Kuhnert, H., Crüger, T., and Pätzold, J.: NAO signature in a Bermuda coral Sr/Ca record, Geochemistry, Geophys. Geosystems, 6, doi:10.1029/2004GC000786, 2005.

Langton, S. J., Linsley, B. K., Robinson, R. S., Rosenthal, Y., Oppo, D. W., Eglinton, T. I., Howe, S. S., Djajadihardja, Y. S., and Syamsudin, F.: 3500 yr record of centennial-scale climate variability from the Western Pacific Warm Pool, Geology, 36, 795–798, doi:10.1130/G24926A.1, 2008.

Lewis, S. C. and LeGrande, A. N.: Stability of ENSO and its tropical Pacific teleconnections over the Last Millennium, Clim. Past, 11, 1347–1360, doi:10.5194/cp-11-1347-2015, 2015.

Li, J., Xie, S.-P., Cook, E. R., Morales, M. S., Christie, D. A., Johnson, N. C., Chen, F., D'Arrigo, R., Fowler, A. M., Gou, X., and Fang, K.: El Niño modulations over the past seven centuries, Nat. Clim. Chang., 3, 822–826, doi:10.1038/nclimate1936, 2013.

Linsley, B. K., Dunbar, R. B., Wellington, G. M., and Mucciarone, D. A.: A coral-based reconstruction of Intertropical Convergence Zone variability over Central America since 1707, J. Geophys. Res., 99, 9977–9994, doi:10.1029/94JC00360, 1994.

Linsley, B. K., Ren, L., Dunbar, R. B., and Howe, S. S.: El Niño Southern Oscillation (ENSO) and decadal-scale climate variability at 10°N in the eastern Pacific from 1893 to 1994: A coral-based reconstruction from Clipperton Atoll, Paleoceanography, 15, 322–335, doi:10.1029/1999PA000428, 2000.

Linsley, B. K., Kaplan, A., Gouriou, Y., Salinger, J., DeMenocal, P. B., Wellington, G. M., and Howe, S. S.: Tracking the extent of the South Pacific Convergence Zone since the early 1600s, Geochemistry, Geophys. Geosystems, 7, 1–15, doi:10.1029/2005GC001115, 2006.

MacDonald, G. M. and Case, R. A.: Variations in the Pacific Decadal Oscillation over the past millennium, Geophys. Res. Lett., 32, 1–4, doi:10.1029/2005GL022478, 2005.

Makou, M. C., Eglinton, T. I., Oppo, D. W., and Hughen, K. A.: Postglacial changes in El Niño and La Niña behavior, Geology, 38, 43–46, doi:10.1130/G30366.1, 2010.

Mann, M. E.: Climate reconstruction using 'Pseudoproxies', Geophys. Res. Lett., 29, 10–13, doi:10.1029/2001GL014554, 2002.

Mann, M. E., Cane, M. A., Zebiak, S. E., and Clement, A. C.: Volcanic and solar forcing of the tropical Pacific over the past 1000 years, J. Clim., 18, 447–456, doi:10.1175/JCLI-3276.1, 2005.

Mann, M. E., Zhang, Z., Hughes, M. K., Bradley, R. S., Miller, S. K., Rutherford, S., and Ni, F.: Proxy-based reconstructions of hemispheric and global surface temperature variations over the past two millennia., Proc. Natl. Acad. Sci. U. S. A., 105, 13 252–13 257, doi:10.1073/pnas.0805721105, 2008.

Mann, M. E., Zhang, Z., Rutherford, S., Bradley, R. S., Hughes, M. K., Shindell, D., Ammann, C., Faluvegi, G., and Ni, F.: Global signatures and dynamical origins of the Little Ice Age and Medieval Climate Anomaly., Science, 326, 1256–1260, doi:10.1126/science.1177303, 2009.

Marchitto, T. M., Muscheler, R., Ortiz, J. D., Carriquiry, J. D., and van Geen, A.: Dynamical response of the tropical Pacific Ocean to solar forcing during the early Holocene., Science, 330, 1378–1381, doi:10.1126/science.1194887, 2010.

Masson-Delmotte, V., Schulz, M., Abe-Ouchi, A., Beer, J., Ganopolski, A., González Rouco, J. F., Jansen, E., Lambeck, K., Luterbacher, J., Naish, T., Osborn, T., Otto-Bliesner, B., Quinn, T., Ramesh, R., Rojas, M., Shao, X., Timmermann, A., and Rouco, J. F. G.: Information from Paleoclimate Archives, in: Clim. Chang. 2013 Phys. Sci. Basis. Contrib. Work. Gr. I to Fifth Assess. Rep. Intergov. Panel Clim. Chang., edited by Stocker, T., Qin, D., Plattner, G.-K., Tignor, M., Allen, S. K., Boschung, J., Nauels, A., Xia, Y., Bex, V., and Midgley, P., pp. 383–464, Cambridge University Press, Cambridge, United Kingdom and New York, NY, USA, doi:10.1017/CBO9781107415324, 2013.

Maupin, C. R., Partin, J. W., Shen, C.-C., Quinn, T. M., Lin, K., Taylor, F. W., Banner, J. L., Thirumalai, K., and Sinclair, D. J.: Persistent decadal-scale rainfall variability in the tropical South Pacific Convergence Zone through the past six centuries, Clim. Past, 10, 1319–1332, doi:10.5194/cp-10-1319-2014, 2014.

McCulloch, M., Mortimer, G., Esat, T., Xianhua, L., Pillans, B., and Chappell, J.: High resolution windows into early Holocene climate: Sr/Ca coral records from the Huon Peninsula, Earth Planet. Sci. Lett., 138, 169–178, doi:10.1016/0012-821X(95)00230-A, 1996.

McGregor, H. V., Gagan, M. K., McCulloch, M. T., Hodge, E., and Mortimer, G.: Mid-Holocene variability in the marine ^{14}C reservoir age for northern coastal Papua New Guinea, Quat. Geochronol., 3, 213–225, doi:10.1016/j.quageo.2007.11.002, 2008.

1215   Medina-Elizalde, M., Burns, S. J., Lea, D. W., Asmerom, Y., von Gunten, L., Polyak, V., Vuille, M., and Kar-malkar, A.: High resolution stalagmite climate record from the Yucatán Peninsula spanning the Maya termi-nal classic period, Earth Planet. Sci. Lett., 298, 255–262, doi:10.1016/j.epsl.2010.08.016, 2010.

Metcalfe, S., Jones, M., Davies, S., Noren, A., and MacKenzie, A.: Climate variability over the last two millenia in the North American Monsoon region, recorded in laminated lake sediments from Labuna de Juanacatlán,
1220   Mexico, The Holocene, 20, 1195–1206, doi:10.1177/0959683610371994, 2010.

Moustafa, Y. A.: Paleoclimatic reconstructions of the northern Red Sea during the Holocene inferred from stable isotope records of modern and fossil corals and molluscs, Berichte aus dem Fachbereich Geowissenschaften, Univ. Bremen, pp. 1–102, 2000.

Moy, A. D., Seltzer, G. O., Rodbell, D. T., and Andersons, D. M.: Variability of El Niño/Southern
1225   Oscillation activity at millennial timescales during the Holocene epoch, Nature, 420, 162–165, doi:doi:10.1038/nature01194, 2002.

Nakamura, N., Kayanne, H., Iijima, H., McClanahan, T. R., Behera, S. K., and Yamagata, T.: Mode shift in the Indian Ocean climate under global warming stress, Geophys. Res. Lett., 36, 3–7, doi:10.1029/2009GL040590, 2009.

1230   Nelson, D. B., Abbott, M. B., Steinman, B., Polissar, P. J., Stansell, N. D., Ortiz, J. D., Rosenmeier, M. F., Finney, B. P., and Riedel, J.: Drought variability in the Pacific Northwest from a 6,000-yr lake sediment record., Proc. Natl. Acad. Sci. U. S. A., 108, 3870–3875, doi:10.1073/pnas.1009194108, 2011.

Newman, M., Compo, G. P., and Alexander, M. A.: ENSO-forced variability of the Pacific Decadal Oscillation, J. Clim., 16, 3853–3857, doi:10.1175/1520-0442(2003)016<3853:EVOTPD>2.0.CO;2, 2003.

1235   Nurhati, I. S., Cobb, K. M., Charles, C. D., and Dunbar, R. B.: Late 20th century warming and freshening in the central tropical Pacific, Geophys. Res. Lett., 36, 1–4, doi:10.1029/2009GL040270, 2009.

Oppo, D. W., Rosenthal, Y., and Linsley, B. K.: 2,000-year-long temperature and hydrology reconstructions from the Indo-Pacific warm pool., Nature, 460, 1113–1116, doi:10.1038/nature08233, 2009.

Page, S. E., Siegert, F., Rieley, J. O., Boehm, H.-D. V., Jaya, A., and Limin, S.: The amount of carbon released
1240   from peat and forest fires in Indonesia during 1997., Nature, 420, 61–65, doi:10.1038/nature01131, 2002.

Partin, J. W., Cobb, K. M., Adkins, J. F., Clark, B., and Fernandez, D. P.: Millennial-scale trends in west Pacific warm pool hydrology since the Last Glacial Maximum., Nature, 449, 452–455, doi:10.1038/nature08125, 2007.

Partin, J. W., Quinn, T. M., Shen, C. C., Emile-Geay, J., Taylor, F. W., Maupin, C. R., Lin, K., Jackson, C. S.,
1245   Banner, J. L., Sinclair, D. J., and Huh, C. A.: Multidecadal rainfall variability in south pacific convergence zone as revealed by stalagmite geochemistry, Geology, 41, 1143–1146, doi:10.1130/G34718.1, 2013.

Pfeiffer, M., Timm, O., Dullo, W. C., and Podlech, S.: Oceanic forcing of interannual and multidecadal climate variability in the southwestern Indian Ocean: Evidence from a 160 year coral isotopic record (La Réunion, 55°E, 21°S), Paleoceanography, 19, 1–14, doi:10.1029/2003PA000964, 2004.

1250   Pohl, K., Therrell, M. D., Blay, G. S., Ayotte, N., Hernandez, J. J. C., Castro, S. D., Oviedo, E. C., Elvir, J. A., Elizondo, M. G., Opland, D., Park, J., Pederson, G., Salazar, S. B., Selem, L. V., Villanueva-Diaz, J., and Stahle, D. W.: A cool season precipitation reconstruction for Satillo, Mexico, Tree-ring Res., 95, 11–19, 2003.

Power, S., Delage, F., Chung, C., Kociuba, G., and Keay, K.: Robust twenty-first-century projections of El Niño and related precipitation variability., Nature, 502, 541–5, doi:10.1038/nature12580, 2013.

Powers, L. A., Johnson, T. C., Werne, J. P., Castañeda, I. S., Hopmans, E. C., Sinninghe Damsté, J. S., and Schouten, S.: Organic geochemical records of environmental variability in Lake Malawi during the last 700 years, Part I: The TEX86 temperature record, Palaeogeogr. Palaeoclimatol. Palaeoecol., 303, 133–139, doi:10.1016/j.palaeo.2010.09.006, 2011.

Quinn, T. M., Crowley, T. J., and Taylor, F. W.: New stable isotope results from a 173-year coral from Espiritu Santo, Vanuatu, Geophys. Res. Lett., 23, 3413–3416, doi:10.1029/96GL03169, 1996.

Quinn, T. M., Crowley, T. J., Taylor, F. W., Henin, C., Joannot, P., and Join, Y.: A multicentury stable isotope record from a New Caledonia coral: Interannual and decadal sea surface temperature variability in the southwest Pacific since 1657 A.D, Paleoceanography, 13, 412–426, doi:doi:10.1029/98PA00401, 1998.

Quinn, T. M., Taylor, F. W., and Crowley, T. J.: Coral-based climate variability in the Western Pacific Warm Pool since 1867, J. Geophys. Res., 111, 1–11, doi:10.1029/2005JC003243, 2006.

Raible, C. C., Lehner, F., González-Rouco, J. F., and Fernández-Donado, L.: Changing correlation structures of the Northern Hemisphere atmospheric circulation from 1000 to 2100 AD, Clim. Past, 10, 537–550, doi:10.5194/cp-10-537-2014, 2014.

Rasbury, M. and Aharon, P.: ENSO-controlled rainfall variability records archived in tropical stalagmites from the mid-ocean island of Niue, South Pacific, Geochemistry, Geophys. Geosystems, 7, doi:10.1029/2005GC001232, 2006.

Reuter, J., Stott, L., Khider, D., Sinha, A., Cheng, H., and Edwards, R. L.: A new perspective on the hydroclimate variability in northern South America during the Little Ice Age, Geophys. Res. Lett., 36, 1–5, doi:10.1029/2009GL041051, 2009.

Richey, J. N., Poore, R. Z., Flower, B. P., Quinn, T. M., and Hollander, D. J.: Regionally coherent Little Ice Age cooling in the Atlantic Warm Pool, Geophys. Res. Lett., 36, 3–7, doi:10.1029/2009GL040445, 2009.

Rodbell, D. T.: An 15,000-Year Record of El Niño-Driven Alluviation in Southwestern Ecuador, Science, 283, 516–520, doi:10.1126/science.283.5401.516, 1999.

Rodysill, J. R., Russell, J. M., Bijaksana, S., Brown, E. T., Safiuddin, L. O., and Eggermont, H.: A paleolimnological record of rainfall and drought from East Java, Indonesia during the last 1,400 years, J. Paleolimnol., 47, 125–139, doi:10.1007/s10933-011-9564-3, 2012.

Russell, J. M. and Johnson, T. C.: Little Ice Age drought in equatorial Africa: Intertropical convergence zone migrations and El Niño-Southern Oscillation variability, Geology, 35, 21–24, doi:10.1130/G23125A.1, 2007.

Russell, J. M., Vogel, H., Konecky, B. L., Bijaksana, S., Huang, Y., Melles, M., Wattrus, N., Costa, K., and King, J. W.: Glacial forcing of central Indonesian hydroclimate since 60,000 y B.P., Proc. Natl. Acad. Sci. U. S. A., 111, 5100–5105, doi:10.1073/pnas.1402373111, 2014.

Russon, T., Tudhope, A. W., Hegerl, G. C., Collins, M., and Tindall, J.: Inter-annual tropical Pacific climate variability in an isotope-enabled CGCM: Implications for interpreting coral stable oxygen isotope records of ENSO, Clim. Past, 9, 1543–1557, doi:10.5194/cp-9-1543-2013, 2013.

Sachs, J. P., Sachse, D., Smittenberg, R. H., Zhang, Z., Battisti, D. S., and Golubic, S.: Southward movement of the Pacific intertropical convergence zone AD 1400–1850, Nat. Geosci., 2, 519–525, doi:10.1038/ngeo554, 2009.

Saenger, C., Cohen, A. L., Oppo, D. W., Halley, R. B., and Carilli, J. E.: Surface-temperature trends and vari-
ability in the low-latitude North Atlantic since 1552, Nat. Geosci., 2, 492–495, doi:10.1038/ngeo552, 2009.

Saenger, C., Came, R. E., Oppo, D. W., Keigwin, L. D., and Cohen, A. L.: Regional climate variabil-
ity in the western subtropical North Atlantic during the past two millennia, Paleoceanography, 26, 1–12,
doi:10.1029/2010PA002038, 2011.

Shin, S. I., Sardeshmukh, P. D., Webb, R. S., Oglesby, R. J., and Barsugli, J. J.: Understanding the mid-Holocene
climate, J. Clim., 19, 2801–2817, doi:10.1175/JCLI3733.1, 2006.

Smerdon, J. E.: Climate models as a test bed for climate reconstruction methods: Pseudoproxy experiments,
Wiley Interdiscip. Rev. Clim. Chang., 3, 63–77, doi:10.1002/wcc.149, 2012.

Stahle, D. W., Diaz, J. V., Burnette, D. J., Paredes, J. C., Heim, R. R., Fye, F. K., Soto, R. A., Therrell, M. D.,
and Cleaveland, M. K.: Major Mesoamerican droughts of the past millennium, Geophys. Res. Lett., 38, 2–5,
doi:10.1029/2010GL046472, 2011.

Stansell, N. D., Steinman, B. A., Abbott, M. B., Rubinov, M., and Roman-Lacayo, M.: Lacustrine stable isotope
record of precipitation changes in Nicaragua during the Little Ice Age and Medieval Climate Anomaly,
Geology, 41, 151–154, doi:10.1130/G33736.1, 2013.

Steinman, B. A., Abbott, M. B., Mann, M. E., Stansell, N. D., and Finney, B. P.: 1,500 year quantitative re-
construction of winter precipitation in the Pacific Northwest, Proc. Natl. Acad. Sci., 109, 11 619–11 623,
doi:10.1073/pnas.1201083109, 2012.

Stott, L., Poulsen, C., Lund, S., and Thunell, R.: Super ENSO and global climate oscillations at millennial time
scales., Science, 297, 222–226, doi:10.1126/science.1071627, 2002.

Stott, L., Cannariato, K., Thunell, R., Haug, G. H., Koutavas, A., and Lund, S.: Decline of surface tem-
perature and salinity in the western tropical Pacific Ocean in the Holocene epoch, Nature, 431, 56–59,
doi:10.1038/nature02903, 2004.

Sturm, C., Zhang, Q., and Noone, D.: An introduction to stable water isotopes in climate models: benefits of
forward proxy modelling for paleoclimatology, Clim. Past, 6, 115–129, doi:10.5194/cpd-5-1697-2009, 2010.

Sundqvist, H. S., Holmgren, K., Fohlmeister, J., Zhang, Q., Matthews, M. B., Spötl, C., and Körnich,
H.: Evidence of a large cooling between 1690 and 1740 AD in southern Africa., Sci. Rep., 3, 1–6,
doi:10.1038/srep01767, 2013.

Swart, P. K., Dodge, R. E., and Hudson, H. J.: A 240-year stable oxygen and carbon isotopic record in a coral
from South Florida: implications for the prediction of precipitation in Southern Florida, Palaios, 11, 362–375,
doi:10.2307/3515246, 1996a.

Swart, P. K., Healy, G., Dodge, R. E., Kramer, P., Hudson, J. H., Halley, R. B., and Robblee, M. B.: The
stable oxygen and carbon isotopic record of climatic and anthropogenic influence., Palaeogeogr., Palaeoclim.,
Palaeoecol., 123, 219–237 [4–5], 1996b.

Takahashi, K., Montecinos, A., Goubanova, K., and Dewitte, B.: ENSO regimes: Reinterpreting the canonical
and Modoki El Niño, Geophys. Res. Lett., 38, 1–5, doi:10.1029/2011GL047364, 2011.

Tan, L., Cai, Y., Cheng, H., An, Z., and Edwards, R. L.: Summer monsoon precipitation variations in cen-
tral China over the past 750 years derived from a high-resolution absolute-dated stalagmite, Palaeogeogr.
Palaeoclimatol. Palaeoecol., 280, 432–439, doi:10.1016/j.palaeo.2009.06.030, 2009.

Taylor, K. E., Stouffer, R. J., and Meehl, G. A.: An overview of CMIP5 and the experiment design, Bull. Am. Meteorol. Soc., 93, 485–498, doi:10.1175/BAMS-D-11-00094.1, 2012.

1335 Thompson, D. M., Ault, T. R., Evans, M. N., Cole, J. E., and Emile-Geay, J.: Comparison of observed and simulated tropical climate trends using a forward model of coral δ^{18}O, Geophys. Res. Lett., 38, 1–6, doi:10.1029/2011GL048224, 2011.

Thompson, L. G. and et Al.: Tropical climate instability: the last glacial cycle from a Qinghai - Tibetan ice core, Science, 276, 1821–1825, doi:10.1126/science.276.5320.1821, 1997.

1340 Thompson, L. G., Mosley-Thompson, E., Davis, M. E., Lin, P.-N. P.-N., Henderson, K. A., Cole-Dai, J., Bolzan, J. F., and Liu, K.-b.: Late Glacial Stage and Holocene Tropical Ice Core Records from Huascaran, Peru, Science, 269, 46–50, doi:10.1017/CBO9781107415324.004, 1995.

Thompson, L. G., Mosley-Thompson, E., Davis, M. E., Henderson, K. A., Brecher, H. H., Zagorodnov, V. S., Mashiotta, T. A., Lin, P.-n., Mikhalenko, V. N., Hardy, D. R., and Beer, J.: Kilimanjaro ice core records: evi-
1345 dence of holocene climate change in tropical Africa., Science, 298, 589–593, doi:10.1126/science.1073198, 2002.

Thompson, L. G., Mosley-Thompson, E., Davis, M. E., Lin, P., Henderson, K., and Mashiotta, T. A.: Tropical glacier and ice core evidence of climate change on annual to millenial time scales, Clim. Change, 59, 137–155, 2003.

1350 Thompson, L. G., Yao, T., Davis, M. E., Mosley-Thompson, E., Mashiotta, T. A., Lin, P. N., Mikhalenko, V. N., and Zagorodnov, V. S.: Holocene climate variability archived in the Puruogangri ice cap on the central Tibetan Plateau, Ann. Glaciol., 43, 61–69, doi:10.3189/172756406781812357, 2006.

Thompson, L. G., Mosley-Thompson, E., Davis, M. E., Zagorodnov, V. S., Howat, I. M., Mikhalenko, V. N., and Lin, P.-N.: Annually resolved ice core records of tropical climate variability over the past ~1800 years.,
1355 Science, 340, 945–950, doi:10.1126/science.1234210, 2013.

Tierney, J. E., Oppo, D. W., Rosenthal, Y., Russell, J. M., and Linsley, B. K.: Coordinated hydro-logical regimes in the Indo-Pacific region during the past two millennia, Paleoceanography, 25, 1–7, doi:10.1029/2009PA001871, 2010.

Tierney, J. E., Lewis, S. C., Cook, B. I., LeGrande, A. N., and Schmidt, G. A.: Model, proxy and
1360 isotopic perspectives on the East African Humid Period, Earth Planet. Sci. Lett., 307, 103–112, doi:10.1016/j.epsl.2011.04.038, 2011.

Tierney, J. E., Abram, N. J., Anchukaitis, K. J., Evans, M. N., Giry, C., Kilbourne, K. H., Saenger, C. P., Wu, H. C., and Zinke, J.: Tropical sea surface temperatures for the past four centuries reconstructed from coral archives, Paleoceanography, 30, 226–252, doi:10.1002/2014PA002717, 2015.

1365 Tiwari, M., Nagoji, S. S., and Ganeshram, R. S.: Multi-centennial scale SST and Indian summer monsoon precipitation variability since mid-Holocene and its nonlinear response to solar activity, The Holocene, 25, 1415–1424, doi:10.1177/0959683615585840, 2015.

Tolwinski-Ward, S. E., Evans, M. N., Hughes, M. K., and Anchukaitis, K. J.: An efficient forward model of the climate controls on interannual variation in tree-ring width, Clim. Dyn., 36, 2419–2439, doi:10.1007/s00382-
1370 010-0945-5, 2011.

39

Treydte, K. S., Schleser, G. H., Helle, G., Frank, D. C., Winiger, M., Haug, G. H., and Esper, J.: The twentieth century was the wettest period in northern Pakistan over the past millennium., Nature, 440, 1179–1182, doi:10.1038/nature04743, 2006.

Trouet, V., Scourse, J. D., and Raible, C. C.: North Atlantic storminess and Atlantic Meridional Overturning

1375   Circulation during the last Millennium: Reconciling contradictory proxy records of NAO variability, Glob. Planet. Change, 84-85, 48–55, doi:10.1016/j.gloplacha.2011.10.003, 2012.

Tudhope, A., Chilcott, C. P., McCulloch, M. T., Cook, E. R., Chappell, J., Ellam, R. M., Lea, D. W., Lough, J. M., and Shimmield, G. B.: Variability in the El Niño-Southern Oscillation through a glacial-interglacial cycle., Science, 291, 1511–1517, doi:10.1126/science.1057969, 2001.

1380   Urban, F. E., Cole, J. E., and Overpeck, J. T.: Influence of mean climate change on climate variability from a 155-year tropical Pacific coral record, Nature, 407, 989–993, doi:10.1038/35039597, 2000.

Vaganov, E. A., Hughes, M. K., and Shashkin, A. V.: Growth Dynamics of Conifer Tree Rings: Images of Past and Future Environments, Springer-Verlag Berlin Heidelberg, New York, 1 edn., doi:10.1007/3-540-31298-6, 2006.

1385   Vaganov, E. A., Anchukaitis, K. J., and Evans, M. N.: How well understood are the processes that create dendroclimatic records? A mechanistic model of the climatic control on conifer tree-ring growth dynamics, in: Dendroclimatology Prog. Prospect., edited by Hughes, M. K., Swetnam, T. W., and Diaz, H. F., vol. 11, pp. 37–75, Springer Netherlands, doi:10.1007/978-1-4020-5725-0, 2011.

van Hengstum, P. J., Donnelly, J. P., Kingston, A. W., Williams, B. E., Scott, D. B., Reinhardt, E. G., Little,

1390   S. N., and Patterson, W. P.: Low-frequency storminess signal at Bermuda linked to cooling events in the North Atlantic region, Paleoceanography, 30, 52–76, doi:doi:10.1002/2014PA002662, 2015.

van Oldenborgh, G. J., Philip, S. Y., and Collins, M.: El Niño in a changing climate : a multi-model study, Ocean Sci., 1, 81–95, doi:10.5194/os-1-81-2005, 2005.

Vasquez-Bedoya, L. F., Cohen, A. L., Oppo, D. W., and Blanchon, P.: Corals record persistent mul-

1395   tidecadal SST variability in the Atlantic Warm Pool since 1775 AD, Paleoceanography, 27, 1–9, doi:10.1029/2012PA002313, 2012.

Vecchi, G. A. and Wittenberg, A. T.: El Niño and our future climate: Where do we stand?, Wiley Interdiscip. Rev. Clim. Chang., 1, 260–270, doi:10.1002/wcc.33, 2010.

Verdon, D. C. and Franks, S. W.: Long-term behaviour of ENSO: Interactions with the PDO over the past 400

1400   years inferred from paleoclimate records, Geophys. Res. Lett., 33, 1–5, doi:10.1029/2005GL025052, 2006.

Wang, H. J., Zhang, R. H., Cole, J. E., and Chavez, F.: El Niño and the related phenomenon Southern Oscillation (ENSO): the largest signal in interannual climate variation., Proc. Natl. Acad. Sci. U. S. A., 96, 11 071–11 072, doi:10.1073/pnas.96.20.11071, 1999.

Wang, J., Emile-Geay, J., Guillot, D., Smerdon, J. E., and Rajaratnam, B.: Evaluating climate field reconstruc-

1405   tion techniques using improved emulations of real-world conditions, Clim. Past, 10, 1–19, doi:10.5194/cp-10-1-2014, 2014.

Wang, J., Emile-Geay, J., Guillot, D., McKay, N. P., and Rajaratnam, B.: Fragility of reconstructed temperature patterns over the Common Era: Implications for model evaluation, Geophys. Res. Lett., 42, 7162–7170, doi:10.1002/2015GL065265, 2015.

40

Wanner, H., Beer, J., Bütikofer, J., Crowley, T. J., Cubasch, U., Flückiger, J., Goosse, H., Grosjean, M., Joos, F., Kaplan, J. O., Küttel, M., Müller, S. A., Prentice, I. C., Solomina, O., Stocker, T. F., Tarasov, P., Wagner, M., and Widmann, M.: Mid- to Late Holocene climate change: an overview, Quat. Sci. Rev., 27, 1791–1828, doi:10.1016/j.quascirev.2008.06.013, 2008.

Wilson, R., Cook, E. R., D'Arrigo, R. D., Riedwyl, N., Evans, M. N., Tudhope, A. W., and Allan, R.: Reconstructing ENSO: the influence of method, proxy data, climate forcing and teleconnections, J. Quat. Sci., 25, 62–78, doi:10.1002/jqs.1297, 2010.

Wolter, K. and Timlin, M. S.: El Niño/Southern Oscillation behaviour since 1871 as diagnosed in an extended multivariate ENSO index (MEI.ext), Int. J. Climatol., 31, 1074–1087, doi:10.1002/joc.2336, 2011.

Wörheide, G.: The reef cave dwelling ultraconservative coralline demosponge Astrosclera willeyana Lister 1900 from the Indo-Pacific, Facies, 38, 1–88, doi:10.1007/BF02537358, 1998.

Wu, H. C., Linsley, B. K., Dassié, E. P., Schiraldi, B., and Demenocal, P. B.: Oceanographic variability in the south pacific convergence zone region over the last 210 years from multi-site coral Sr/Ca records, Geochemistry, Geophys. Geosystems, 14, 1435–1453, doi:10.1029/2012GC004293, 2013.

Wurtzel, J. B., Black, D. E., Thunell, R. C., Peterson, L. C., Tappa, E. J., and Rahman, S.: Mechanisms of southern Caribbean SST variability over the last two millennia, Geophys. Res. Lett., 40, 5954–5958, doi:10.1002/2013GL058458, 2013.

Yan, H., Sun, L., Oppo, D. W., Wang, Y., Liu, Z., Xie, Z., Liu, X., and Cheng, W.: South China Sea hydrological changes and Pacific Walker Circulation variations over the last millennium., Nat. Commun., 2, 293, doi:10.1038/ncomms1297, 2011a.

Yan, H., Sun, L., Wang, Y., Huang, W., Qiu, S., and Yang, C.: A record of the Southern Oscillation Index for the past 2,000 years from precipitation proxies, Nat. Geosci., 4, 611–614, doi:10.1038/ngeo1231, 2011b.

Yeh, S.-W., Kug, J.-S., Dewitte, B., Kwon, M.-H., Kirtman, B. P., and Jin, F.-F.: El Niño in a changing climate, Nature, 461, 511–514, doi:10.1038/nature08316, 2009.

Yi, L., Yu, H., Ge, J., Lai, Z., Xu, X., Qin, L., and Peng, S.: Reconstructions of annual summer precipitation and temperature in north-central China since 1470 AD based on drought/flood index and tree-ring records, Clim. Change, 110, 469–498, doi:10.1007/s10584-011-0052-6, 2012.

Yuan Zhang, Wallace, J. M., and Battisti, D. S.: ENSO-like interdecadal variability: 1900-93, J. Clim., 10, 1004–1020, doi:10.1175/1520-0442(1997)010<1004:ELIV>2.0.CO;2, 1997.

Zhao, M., Read, G., and Schimmelmann, A.: An alkenone ($U_{37}^{K'}$) quasi-annual sea surface temperature record (A.D. 1440 to 1940) using varved sediments from the Santa Barbara Basin, Org. Geochem., 31, 903–917, 2000.

Zinke, J., Dullo, W. C., Heiss, G. A., and Eisenhauer, A.: ENSO and Indian Ocean subtropical dipole variability is recorded in a coral record off southwest Madagascar for the period 1659 to 1995, Earth Planet. Sci. Lett., 228, 177–194, doi:10.1016/j.epsl.2004.09.028, 2004.

Zinke, J., Pfeiffer, M., Timm, O., Dullo, W. C., Kroon, D., and Thomassin, B. A.: Mayotte coral reveals hydrological changes in the western indian ocean between 1881 and 1994, Geophys. Res. Lett., 35, 1–5, doi:10.1029/2008GL035634, 2008.

Zinke, J., Loveday, B. R., Reason, C. J. C., Dullo, W.-C., and Kroon, D.: Madagascar corals track sea surface temperature variability in the Agulhas Current core region over the past 334 years., Sci. Rep., 4, 4393, doi:10.1038/srep04393, 2014.

Zinke, J., Hoell, a., Lough, J. M., Feng, M., Kuret, a. J., Clarke, H., Ricca, V., Rankenburg, K., and McCulloch, M. T.: Coral record of southeast Indian Ocean marine heatwaves with intensified Western Pacific temperature gradient., Nat. Commun., 6, 8562, doi:10.1038/ncomms9562, 2015.

1450
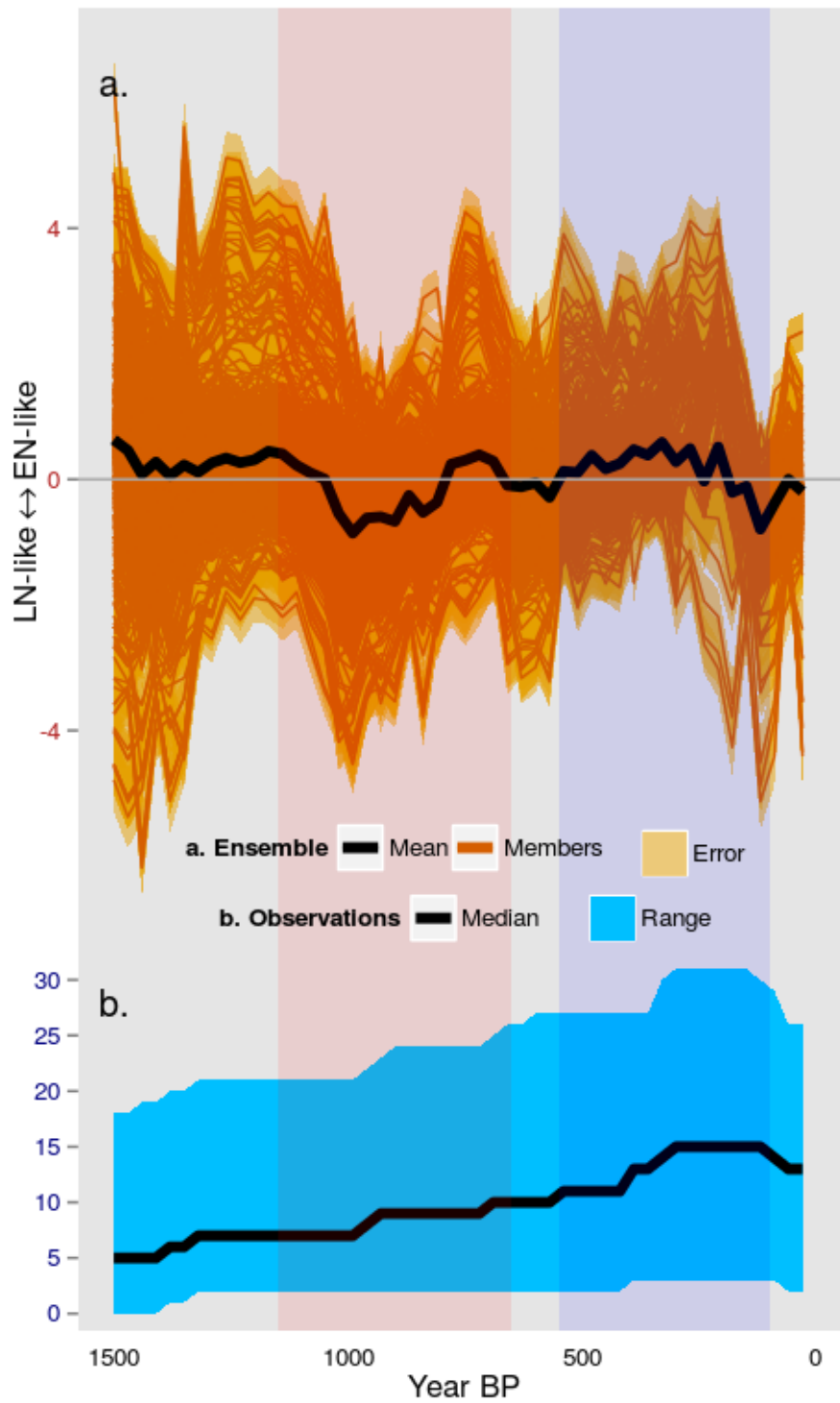
Figure 2. Precipitation ENSO ensembles. a) 30 year averaged precipitation reconstruction of ENSO-like climate change (black line). Individual network solutions are shown as orange lines, with the uncertainty envelope in orange shading. b) Number of proxies included in the ensemble over time, with the median in black and the range in blue. The pink and purple shaded periods are the MCA and LIA respectively.
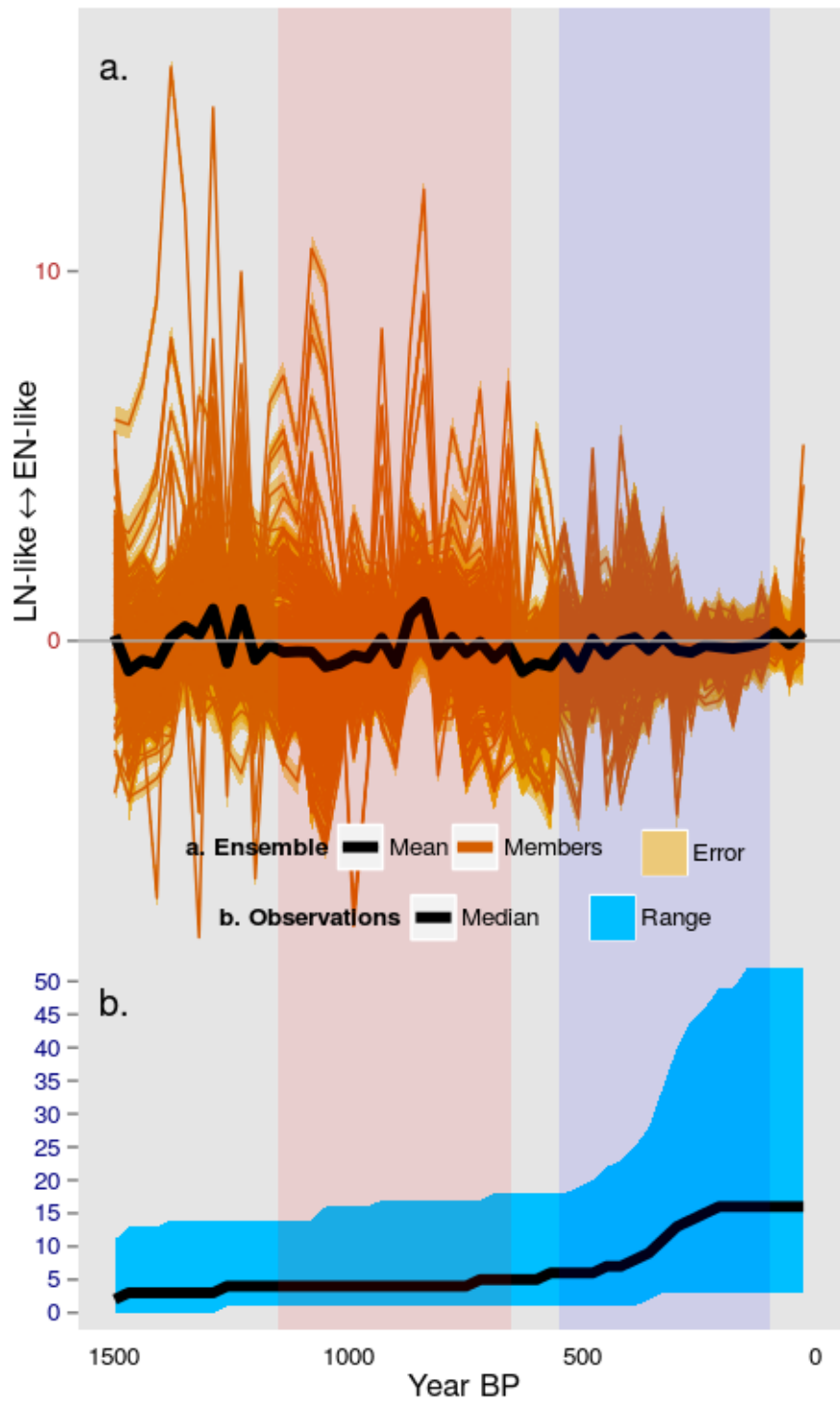
Figure 3. Temperature ENSO ensembles. As Fig. 2, but for temperature.
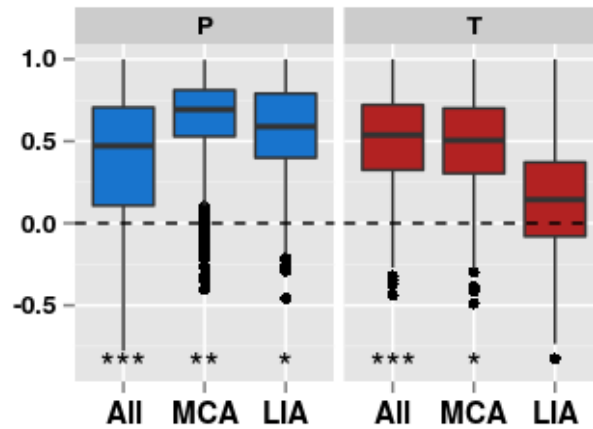
Figure 4. Within-ensemble correlations. Correlations between 1000 pairs randomly chosen from the precipitation (blue) and temperature (red) ensembles. Box plots encapsulate the space between the first and third quartile with the median shown as a black line; whiskers indicate the 95% confidence interval of the median; points are values outside this confidence interval (outliers). Statistical significance of the median value is indicated at the bottom: *** $p < 0.001$, ** $p < 0.01$, * $p < 0.05$, ˆ $p < 0.1$, $p > 0.1$.
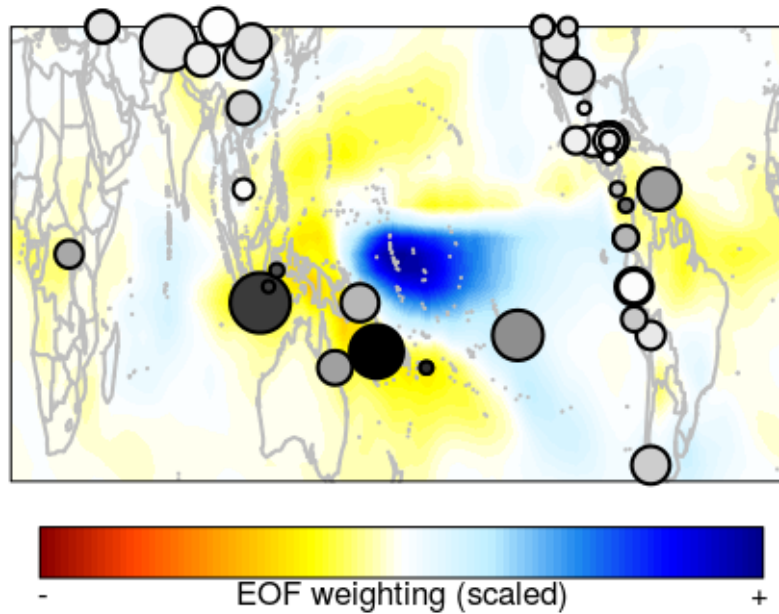
Figure 5. Precipitation EOF with proxy locations. Background colours are scaled EOF values. Bubbles are individual proxies; size is indicative of how often the proxy is included in the network ensemble, shading indicates relative weighting such that darker colours are more strongly positive or negative.
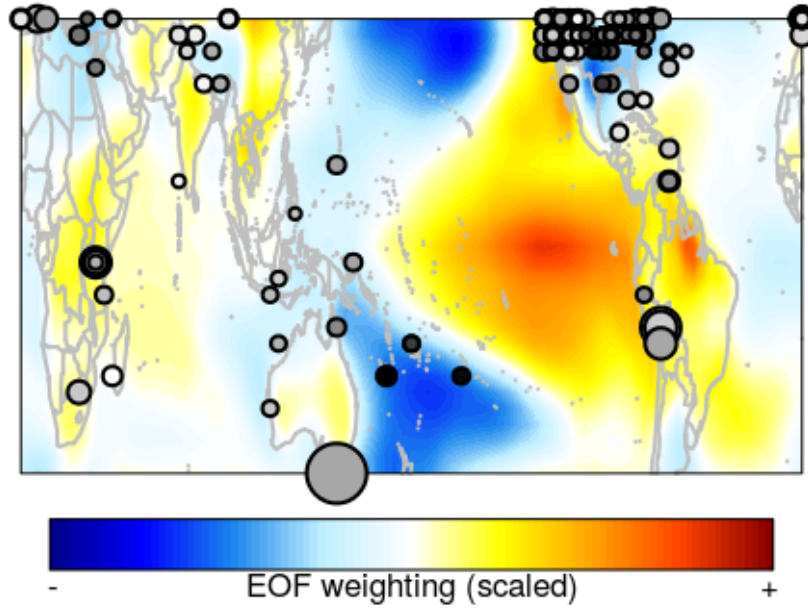
Figure 6. Temperature EOF with proxy locations. As Fig. 5, but for temperature.
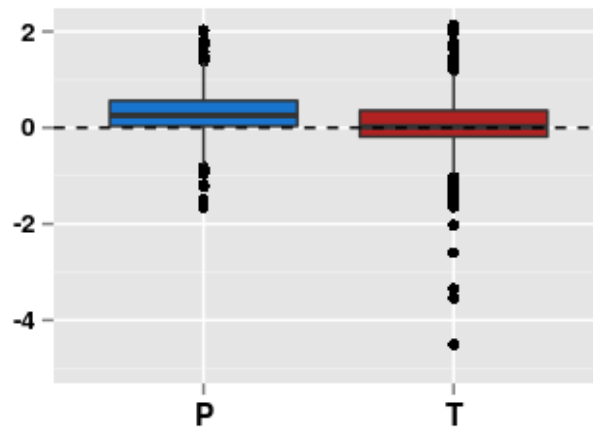
Figure 7. Difference between the means of the MCA and LIA. Difference calculated by subtracting μ_{MCA} from μ_{LIA} for each ensemble member. A positive value indicates LIA is more El Niño-like than MCA. Precipitation is on the left in blue, temperature is on the right in red. See Fig. 4 for explanation of the box plots and significance.

46
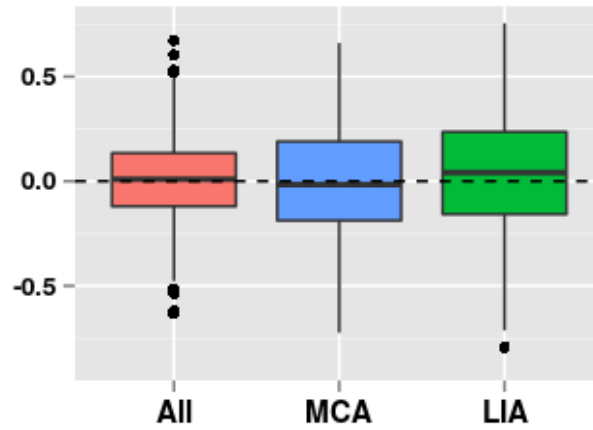
Figure 8. Precipitation – temperature correlations. Correlations between the temperature and precipitation ensemble members based on 1000 randomly chosen pairs, for the period 100-1500 yrBP ('All') and the MCA and LIA individually. See Fig. 4 for explanation of the box plots and significance.
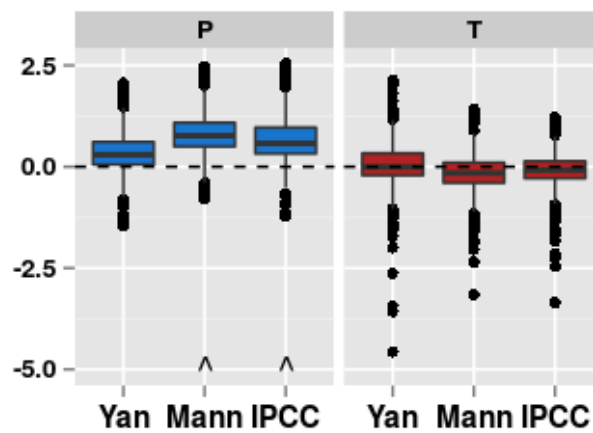
Figure 9. Sensitivity to MCA and LIA definitions. As Fig 7, done for the three MCA and LIA definitions listed in Sect 4. 'Yan' refers to the definition used in Yan et al. (2011b), 'Mann' in Mann et al. (2009), and 'IPCC' in Masson-Delmotte et al. (2013). See Fig. 4 for explanation of the box plots and significance.

Reference	Lon	Lat	Proxy	SNR	EOF	Start	End	Res	Dating	Included?
Anchukaitis and Evans (2010)	275	10	treering	N/A	N/A	50	-53	1	2	No; Length
Anderson (2011)	68	29	lake	0.40	0.32	>1500	-58	14	50	Yes
Apastaégui et al. (2014)	76	13	speleothem	0.40	-0.03	413	22	5	15	Yes
Asmerom et al. (2007)	255	32	speleothem	N/A	N/A	>1500	-15	17	550	No; Dating error
Baker et al. (2009)	78	10	lake	0.40	-0.22	>1500	127	10	30	Yes
Bird et al. (2011)	76	11	lake	0.40	0.52	>1500	-57	20	60	Yes
Bonnefille and Chalié (2000)	356	30	pollen	N/A	N/A	>1500	0	23	110	No; Dating error
Buckley et al. (2010)	29	19	treering	0.37	0.04	920	-58	1	1	Yes
Chen et al. (2009)	26	29	lake	0.40	-0.02	960	-52	10	60	Yes
Christie et al. (2011)	78	2	treering	0.35	0.48	604	-52	1	1	Yes
Cleaveland et al. (2003)	29	24	treering	0.40	0.42	564	-43	1	1	Yes
Conroy et al. (2008) C/N	271	-1	lake	N/A	N/A	>1500	-54	10	70	No; Dating error
Conroy et al. (2008) clay	271	-1	lake	N/A	N/A	>1500	-54	10	70	No; Dating error
Conroy et al. (2008) sand	271	-1	lake	N/A	N/A	>1500	-54	10	70	No; Dating error
Conroy et al. (2008) silt	271	-1	lake	N/A	N/A	>1500	-54	10	70	No; Dating error
Curtis et al. (1996) gastropod	73	22	lake	0.40	0.16	>1500	-43	6	50	Yes
Curtis et al. (1996) ostracod	73	22	lake	0.40	0.16	>1500	-43	6	50	Yes
Denniston et al. (2015)	62	10	speleothem	0.40	1.08	>1500	-36	1	30	Yes
Díaz et al. (2002)	69	26	treering	1.10	0.32	303	-42	1	1	Yes
Faulstich et al. (2013)	67	28	treering	0.46	0.26	353	-58	1	1	Yes
Griffin et al. (2013)	67	27	treering	0.40	0.31	411	-58	1	1	Yes
Haug et al. (2001) Fe	79	19	marine	0.40	-0.93	>1500	110	5	50	Yes
Haug et al. (2001) Ti	79	19	marine	0.40	-0.93	>1500	110	5	50	Yes
Hendy et al. (2003)	40	8	coral	0.86	-0.90	338	-35	1	1	Yes
Hodell et al. (1995) gastropod	73	22	lake	0.40	0.16	>1500	-10	25	60	Yes
Hodell et al. (1995) ostracod	73	22	lake	0.40	0.16	>1500	-10	25	60	Yes
Hodell et al. (1995) s	73	22	lake	0.40	0.16	>1500	157	25	60	Yes
Kennett et al. (2012)	73	21	speleothem	0.40	0.00	>1500	-54	1	19	Yes
Linsley et al. (1994) $\delta^{18}O$	75	18	coral	0.10	-1.38	242	-35	1	1	Yes
Maupin et al. (2014) 10fc	43	12	speleothem	2.35	-0.68	527	-60	1	6	Yes
Maupin et al. (2014) 5fc	160	-10	speleothem	N/A	N/A	70	-26	1	5	No; Length
Medina-Elizalde et al. (2010)	73	22	speleothem	0.79	0.16	1463	-54	2	10	Yes
Metcalfe et al. (2010)	69	22	lake	0.40	-0.16	>1500	-51	1	24	Yes
Moy et al. (2002)	75	16	lake	0.40	0.70	>1500	-27	1	60	Yes
Nelson et al. (2011)	65	29	lake	0.40	0.24	>1500	101	5	60	Yes

1455

Reference	Lon	Lat	Proxy	SNR	EOF	Start	End	Res	Dating	Included?
Table 1 continued from previous page										
Oppo et al. (2009) $\delta^{18}O$sw	32	13	marine	0.40	-1.82	>1500	-5	11	50	Yes
Partin et al. (2007)	115	4	speleothem	N/A	N/A	>1500	0	45	300	No; Dating error
Partin et al. (2013)	45	9	speleothem	1.10	-2.42	393	-55	1	11	Yes
Pohl et al. (2003)	70	24	treering	1.01	0.18	168	-50	1	1	Yes
Rasbury and Aharon (2006) asm1	51	8	speleothem	0.40	-1.97	121	-51	1	7	Yes
Rasbury and Aharon (2006) asm2	51	8	speleothem	0.40	-1.97	190	-51	1	5	Yes
Rasbury and Aharon (2006) asm3	190	-19	speleothem	N/A	N/A	76	-51	1	13	No; Length
Reuter et al. (2009) a	283	-6	speleothem	N/A	N/A	47	-56	1	9	No; Length
Reuter et al. (2009) d	76	13	speleothem	0.40	-0.03	861	43	1	9	Yes
Rodbell (1999) old	75	16	lake	0.40	0.70	>1500	802	1	10	No; AOI
Rodbell (1999) recent	75	16	lake	0.40	0.70	662	-27	1	10	Yes
Rodysill et al. (2012)	31	12	lake	0.40	-1.86	1290	-59	55	60	Yes
Russell et al. (2014) $\delta^{13}C$wax	33	14	lake	0.40	-1.67	>1500	630	220	57	Yes
Russell et al. (2014) TiO	33	14	lake	0.40	-1.67	>1500	669	220	57	No; AOI
Russell and Johnson (2007)	8	15	lake	0.40	-0.83	1399	-24	3	10	Yes
Stahle et al. (2011)	71	22	treering	0.79	0.00	1179	-58	1	1	Yes
Stansell et al. (2013)	74	19	lake	0.40	-0.61	>1500	-54	5	10	Yes
Steinman et al. (2012) Castor	65	29	lake	1.43	0.24	1450	-50	5	60	Yes
Tan et al. (2009)	29	27	speleothem	0.42	-0.27	701	-33	3	8	Yes
Thompson et al. (2006) c2an	24	27	ice core	0.40	-0.16	349	-46	10	50	Yes
Tierney et al. (2010)	120	-4	marine	N/A	N/A	>1500	-48	30	65	No; Dating error
Tierney et al. (2015) bc1δDwax	12	29	marine	0.40	0.24	322	-50	9	25	Yes
Tierney et al. (2015) pδDwax	12	29	marine	0.40	0.24	>1500	-30	20	25	Yes
Treydte et al. (2006)	20	28	treering	0.61	0.22	950	-48	1	1	Yes
Yan et al. (2011a) dy2	113	17	lake	N/A	N/A	926	-46	15	70	No; Dating error
Yan et al. (2011a) dy4	113	17	lake	N/A	N/A	926	-46	20	70	No; Dating error
Yan et al. (2011a) dy6	113	17	lake	N/A	N/A	926	-53	10	70	No; Dating error
Yi et al. (2012)	30	28	treering	0.40	-0.29	350	-50	1	1	Yes

Table 1. Precipitation proxy details. 'SNR' gives the signal-to-noise ratio used to make the pseudoproxies. 'EOF' gives the (unscaled) 20CRV2c EOF value used to weight the proxy. 'Start' and 'End' are starting and ending years in YearBP. 'Res' is proxy resolution, rounded to the nearest integer; sub-annual proxies are listed as having a 1-year resolution. 'Dating' refers to dating error. 'Included?' indicates whether the proxy contributed to the final ENSO reconstruction; if not, the reason for exclusion is listed ('Dating error' and 'Length' are *a priori* conditions which the proxies failed to meet. 'AOI' indicates it passed pre-processing screening, but was not selected during the add-one-in process).

Reference	Lon	Lat	Proxy	SNR	EOF	Start	End	Res	Dating	Included?
Alibert and Kinsley (2008) Sr/Ca	151	-3	coral	0.26	-0.73	127	-47	1	1	Yes
ar018	266	35	treering	0.40	-1.63	300	-29	1	1	Yes
ar024	266	36	treering	0.40	-1.07	225	-29	1	1	Yes
ar030	267	35	treering	0.40	-1.42	214	-29	1	1	Yes
ar042	268	35	treering	0.40	-1.42	428	-29	1	1	Yes
ar048	269	36	treering	0.40	-0.94	533	-29	1	1	Yes
ar050	269	35	treering	0.40	-0.94	931	-30	1	1	Yes
ar055	267	36	treering	0.40	-0.94	591	-42	1	1	Yes
ar056	267	36	treering	0.40	-0.94	280	-42	1	1	Yes
ar057	267	36	treering	0.40	-0.94	330	-43	1	1	Yes
ar058	266	36	treering	0.40	-1.07	271	-42	1	1	Yes
ar060	268	36	treering	0.40	-0.94	313	-43	1	1	Yes
ar061	267	37	treering	0.40	-0.94	258	-43	1	1	Yes
ar064	266	34	treering	0.40	-1.63	292	-41	1	1	Yes
ar072	266	36	treering	0.40	-1.07	325	-41	1	1	Yes
Asami (2005) $\delta^{18}O$	145	13	coral	0.71	-0.76	160	-50	1	1	Yes
aust002	11	47	treering	0.40	-0.56	384	-21	1	1	Yes
az080	251	36	treering	0.40	0.42	352	-21	1	1	Yes
az081	251	36	treering	0.40	0.42	349	-21	1	1	Yes
az082	251	36	treering	0.40	0.42	574	-22	1	1	Yes
az084	250	36	treering	0.40	0.42	480	-21	1	1	Yes
az086	249	37	treering	0.40	0.42	585	-21	1	1	Yes
az089	250	34	treering	0.40	0.20	354	-22	1	1	Yes
az091	248	36	treering	0.40	0.42	261	-22	1	1	Yes
az098	248	36	treering	0.40	0.42	302	-22	1	1	Yes
az099	250	35	treering	0.40	0.20	263	-23	1	1	Yes
az102	250	37	treering	0.40	0.42	460	-22	1	1	Yes
az104	246	37	treering	0.40	0.51	356	-21	1	1	Yes
az106	248	36	treering	0.40	0.42	502	-25	1	1	Yes
az109	247	35	treering	0.40	0.51	352	-21	1	1	Yes
az127	248	37	treering	0.40	0.42	369	-26	1	1	Yes
az129	248	37	treering	0.40	0.42	468	-26	1	1	Yes
az135	246	35	treering	0.40	0.51	381	-21	1	1	Yes
az143	247	36	treering	0.40	0.51	307	-22	1	1	Yes
az144	248	37	treering	0.40	0.42	469	-25	1	1	Yes

Reference	Lon	Lat	Proxy	SNR	EOF	Start	End	Res	Dating	Included?
Table 2 continued from previous page										
az505	248	36	treering	0.40	0.42	257	-25	1	1	Yes
az510	248	36	treering	0.40	0.42	1402	-33	1	1	Yes
az527	249	34	treering	0.40	0.20	320	-36	1	1	Yes
az542	250	34	treering	0.40	0.20	320	-36	1	1	Yes
Bagnato et al. (2005) $\delta^{18}O$	179	-17	coral	0.16	-1.56	174	-51	1	1	Yes
Barron (2003)	235	42	marine	N/A	N/A	15804	158	100	90	No; Dating error
Berke et al. (2012)	37	3	lake	N/A	N/A	173	-40	6	6	No; AOI
Berke et al. (2012)	37	3	lake	N/A	N/A	2529	477	44	60	No; AOI
Black et al. (2007)	295	11	marine	0.40	0.89	729	-40	2	5	Yes
Boiseau et al. (1999) $\delta^{18}O$	210	-18	coral	N/A	N/A	98	-41	1	1	No; Length
ca051	243	34	treering	0.40	0.90	1992	-20	1	1	Yes
ca066	239	40	treering	0.40	0.40	479	-30	1	1	Yes
ca067	239	40	treering	0.40	0.40	466	-30	1	1	Yes
ca089	242	35	treering	0.40	0.39	445	-31	1	1	Yes
ca092	241	37	treering	0.40	0.39	516	-31	1	1	Yes
ca094	242	36	treering	0.40	0.39	422	-31	1	1	Yes
ca514	242	36	treering	0.40	0.39	343	-31	1	1	Yes
ca528	242	37	treering	0.40	0.39	1052	-37	1	1	Yes
ca529	241	37	treering	0.40	0.39	1251	-37	1	1	Yes
ca530	242	37	treering	0.40	0.39	1033	-37	1	1	Yes
ca531	242	37	treering	0.40	0.39	923	-37	1	1	Yes
ca532	241	37	treering	0.40	0.39	900	-37	1	1	Yes
ca536	243	34	treering	0.40	0.90	296	-38	1	1	Yes
ca544	243	34	treering	0.40	0.90	243	-38	1	1	Yes
ca546	243	34	treering	0.40	0.90	209	-38	1	1	Yes
ca547	243	34	treering	0.40	0.90	266	-38	1	1	Yes
ca552	243	34	treering	0.40	0.90	322	-38	1	1	Yes
ca555	237	40	treering	0.40	0.40	773	-38	1	1	Yes
ca609	243	34	treering	0.40	0.90	390	-45	1	1	Yes
ca612	241	35	treering	0.40	0.90	480	-43	1	1	Yes
ca619	238	40	treering	0.40	0.40	587	-54	1	1	Yes
ca621	241	36	treering	0.40	0.39	365	-53	1	1	Yes
ca625	239	37	treering	0.40	0.63	440	-53	1	1	Yes
ca626	239	37	treering	0.40	0.63	373	-53	1	1	Yes
ca628	239	40	treering	0.40	0.40	500	-48	1	1	Yes
Charles (1997) $\delta^{18}O$	55	-5	coral	0.71	0.25	103	-45	1	1	No; AOI
										Table 2 continued on next page

Table 2 continued from previous page

Reference	Lon	Lat	Proxy	SNR	EOF	Start	End	Res	Dating	Included?
Charles et al. (2003) Bali	116	-8	coral	0.46	-0.55	168	-40	1	1	Yes
Charles et al. (2003) Bunaken	125	2	coral	N/A	N/A	90	-41	1	1	No; Length
co066	252	38	treering	0.40	-0.29	493	-28	1	1	Yes
co067	252	38	treering	0.40	-0.29	680	-28	1	1	Yes
co511	254	40	treering	0.40	0.02	781	-39	1	1	Yes
co526	255	40	treering	0.40	0.02	300	-30	1	1	Yes
co532	254	40	treering	0.40	0.02	310	-37	1	1	Yes
co533	255	40	treering	0.40	0.02	400	-37	1	1	Yes
co538	255	41	treering	0.40	0.02	280	-37	1	1	Yes
co542	255	40	treering	0.40	0.02	260	-37	1	1	Yes
co543	254	40	treering	0.40	0.02	380	-37	1	1	Yes
co544	254	40	treering	0.40	0.02	520	-37	1	1	Yes
co545	255	40	treering	0.40	0.02	620	-37	1	1	Yes
co547	254	40	treering	0.40	0.02	880	-37	1	1	Yes
co548	255	39	treering	0.40	-0.79	300	-38	1	1	Yes
co549	254	40	treering	0.40	0.02	440	-37	1	1	Yes
co550	255	40	treering	0.40	0.02	260	-37	1	1	Yes
co551	255	40	treering	0.40	0.02	200	-37	1	1	Yes
co563	254	40	treering	0.40	0.02	252	-51	1	1	Yes
co568	257	37	treering	0.40	-1.27	322	-48	1	1	Yes
co569	256	37	treering	0.40	-1.27	486	-47	1	1	Yes
co572	255	40	treering	0.40	0.02	1056	-48	1	1	Yes
co579	254	40	treering	0.40	0.02	630	-52	1	1	Yes
co581	253	41	treering	0.40	0.02	411	-50	1	1	Yes
Cole (2000)	40	-3	coral	N/A	N/A	149	-44	1	1	No; AOI
Conroy et al. (2009)	271	-1	lake	N/A	N/A	1219	-54	5	70	No; Dating error
Cook et al. (2000)	146	-42	treering	0.53	-0.71	3550	-41	1	1	Yes
Cronin et al. (2003)	284	38	marine	N/A	N/A	2134	-45	8	80	No; Dating error
Cronin et al. (2005)	284	38	marine	N/A	N/A	2127	-45	8	80	No; Dating error
Damassa et al. (2006) $\delta^{18}O$	40	-8	coral	0.66	0.54	328	-48	1	5	Yes
DeLong et al. (2012)	167	-23	coral	0.61	-2.06	301	-50	1	1	Yes
DeLong et al. (2014)	277	25	coral	0.93	-0.57	216	-59	1	1	Yes
Dunbar et al. (1994)	269	0	coral	N/A	N/A	343	-31	1	1	No; AOI
Felis et al. (2010) UCa	142	27	coral	N/A	N/A	77	-44	1	1	No; Length
Goni et al. (2006) Cariaco	295	11	marine	0.40	0.89	256	-46	8	60	Yes
Goni et al. (2006) Guaymas	248	28	marine	0.40	0.79	223	-38	5	60	Yes

1460

52

Table 2 continued from previous page

Reference	Lon	Lat	Proxy	SNR	EOF	Start	End	Res	Dating	Included?
Goodkin et al. (2008)	296	32	coral	0.40	-0.45	168	-48	1	1	Yes
Guilderson and Schrag (1999) $\delta^{18}O$	166	-30	coral	N/A	N/A	53	-46	1	1	No; Length
Heiss (1994)	35	29	coral	0.29	-1.06	161	-43	1	1	Yes
Hetzinger et al. (2010) $\delta^{18}O$	-422	16	coral	N/A	N/A	54	-49	1	1	No; Length
Hetzinger et al. (2010) Sr/Ca	-422	16	coral	N/A	N/A	54	-49	1	1	No; Length
ia003	268	41	treering	0.40	-0.41	235	-31	1	1	Yes
id002	244	48	treering	0.40	0.63	278	-26	1	1	Yes
il010	270	40	treering	0.40	-0.55	279	-30	1	1	Yes
il011	272	39	treering	0.40	-0.55	276	-30	1	1	Yes
il013	271	38	treering	0.40	-0.99	295	-31	1	1	Yes
il014	271	38	treering	0.40	-0.99	298	-31	1	1	Yes
indi002	74	35	treering	0.40	-0.23	346	-30	1	1	Yes
indi006	76	35	treering	0.40	-0.34	296	-31	1	1	Yes
ital023	12	47	treering	0.40	-0.75	476	-40	1	1	Yes
Keigwin (1996)	302	34	marine	0.77	-0.41	3125	25	50	50	Yes
Kellerhals et al. (2010)	292	-17	ice core	0.40	0.71	1595	-45	10	20	Yes
Khider et al. (2014) SST	126	7	marine	N/A	N/A	9960	199	15	262	No; Dating error
Kilbourne et al. (2008) $\delta^{18}O$	293	18	coral	0.30	0.47	199	-54	1	1	Yes
Krusic et al. (2015)	91	27	treering	0.40	-0.66	574	-63	1	1	Yes
ks007	264	38	treering	0.40	-1.07	212	-29	1	1	Yes
Kuhnert et al. (2000)	114	-22	coral	N/A	N/A	71	-45	1	1	No; AOI
Kuhnert et al. (2005) $\delta^{18}O$	295	33	coral	0.11	-0.77	83	-33	1	1	Yes
ky003	277	37	treering	0.40	-1.12	290	-32	1	1	Yes
Linsley et al. (2000) Clipperton	251	10	coral	N/A	N/A	55	-44	1	1	No; Length
Linsley et al. (2006) Rarotonga Sr/Ca	201	-22	coral	0.15	-1.99	223	-47	1	1	Yes
Linsley et al. (2006) Savusavu Sr/Ca	179	-17	coral	0.28	-1.56	168	-47	1	1	Yes
Marchitto et al. (2010)	247	25	marine	0.40	2.06	13812	832	50	50	No; AOI
me019	292	46	treering	0.40	-0.80	253	-31	1	1	Yes
mi009	275	47	treering	0.40	-0.83	440	-33	1	1	Yes
mo003	269	37	treering	0.40	-0.94	257	-31	1	1	Yes
mo005	270	38	treering	0.40	-0.94	242	-32	1	1	Yes
mo018	266	37	treering	0.40	-1.07	226	-29	1	1	Yes
mo033	267	37	treering	0.40	-0.94	254	-42	1	1	Yes
mo036	266	37	treering	0.40	-1.07	261	-29	1	1	Yes
mo037	270	37	treering	0.40	-0.94	765	-42	1	1	Yes
mo038	268	37	treering	0.40	-0.94	397	-42	1	1	Yes

Table 2 continued from previous page

Reference	Lon	Lat	Proxy	SNR	EOF	Start	End	Res	Dating	Included?
mo039	268	38	treering	0.40	-0.94	286	-42	1	1	Yes
mo040	269	37	treering	0.40	-0.94	257	-43	1	1	Yes
mo043	269	37	treering	0.40	-0.94	812	-40	1	1	Yes
morc002	355	35	treering	0.40	0.34	318	-34	1	1	Yes
Moustafa (2000)	34	28	coral	N/A	N/A	52	-43	1	1	No; Length
nc002	277	36	treering	0.40	-1.12	392	-33	1	1	Yes
nc003	278	36	treering	0.40	-1.09	390	-33	1	1	Yes
nc006	277	35	treering	0.40	-1.12	273	-33	1	1	Yes
nc007	278	36	treering	0.40	-1.09	333	-27	1	1	Yes
nc009	283	37	treering	0.40	-1.11	426	-34	1	1	Yes
nj001	285	41	treering	0.40	-0.76	330	-32	1	1	Yes
nj002	285	41	treering	0.40	-0.76	276	-32	1	1	Yes
nm021	252	37	treering	0.40	-0.29	395	-21	1	1	Yes
nm023	252	37	treering	0.40	-0.29	375	-21	1	1	Yes
nm024	253	37	treering	0.40	-0.29	307	-21	1	1	Yes
nm025	252	36	treering	0.40	-0.29	569	-22	1	1	Yes
nm026	254	36	treering	0.40	-0.29	588	-22	1	1	Yes
nm031	252	35	treering	0.40	-0.29	472	-22	1	1	Yes
nm033	252	35	treering	0.40	-0.29	414	-22	1	1	Yes
nm034	252	35	treering	0.40	-0.52	288	-22	1	1	Yes
nm038	254	36	treering	0.40	-0.29	394	-22	1	1	Yes
nm040	254	36	treering	0.40	-0.29	371	-22	1	1	Yes
nm047	257	37	treering	0.40	-1.27	310	-24	1	1	Yes
nm051	253	36	treering	0.40	-0.29	263	-26	1	1	Yes
nm053	252	36	treering	0.40	-0.29	321	-26	1	1	Yes
nm055	253	37	treering	0.40	-0.29	356	-21	1	1	Yes
nm118	254	35	treering	0.40	-0.29	386	-32	1	1	Yes
nm500	254	36	treering	0.40	-0.29	242	-22	1	1	Yes
nm501	254	36	treering	0.40	-0.29	223	-22	1	1	Yes
nm529	251	36	treering	0.40	0.42	298	-27	1	1	Yes
nm548	255	37	treering	0.40	-0.29	358	-31	1	1	Yes
nm549	255	37	treering	0.40	-0.29	311	-37	1	1	Yes
nm550	253	36	treering	0.40	-0.29	418	-36	1	1	Yes
nm551	255	36	treering	0.40	-0.29	250	-31	1	1	Yes
nm552	255	36	treering	0.40	-0.29	369	-31	1	1	Yes
nm554	255	36	treering	0.40	-0.29	260	-36	1	1	Yes

Table 2 continued from previous page

Reference	Lon	Lat	Proxy	SNR	EOF	Start	End	Res	Dating	Included?
nm555	253	36	treering	0.40	-0.29	346	-36	1	1	Yes
nm556	253	36	treering	0.40	-0.29	378	-36	1	1	Yes
nm557	254	36	treering	0.40	-0.29	395	-36	1	1	Yes
nm558	253	36	treering	0.40	-0.29	297	-37	1	1	Yes
nm559	255	37	treering	0.40	-0.29	559	-37	1	1	Yes
nm560	255	37	treering	0.40	-0.29	1113	-39	1	1	Yes
nm575	256	37	treering	0.40	-1.27	238	-48	1	1	Yes
nm576	256	37	treering	0.40	-1.27	324	-48	1	1	Yes
nm577	256	36	treering	0.40	-1.27	355	-48	1	1	Yes
Nurhati et al. (2009)	198	6	coral	N/A	N/A	64	-48	1	1	No; AOI
nv048	245	40	treering	0.40	0.63	447	-28	1	1	Yes
nv506	245	37	treering	0.40	0.51	345	-27	1	1	Yes
nv507	245	39	treering	0.40	0.63	485	-26	1	1	Yes
nv509	245	39	treering	0.40	0.63	399	-26	1	1	Yes
nv510	244	36	treering	0.40	0.51	1150	-34	1	1	Yes
nv512	245	40	treering	0.40	0.63	1630	-35	1	1	Yes
nv513	246	39	treering	0.40	0.63	1125	-33	1	1	Yes
nv514	245	41	treering	0.40	0.63	1648	-35	1	1	Yes
nv516	246	39	treering	0.40	0.63	1950	-34	1	1	Yes
nv517	244	36	treering	0.40	0.51	1630	-34	1	1	Yes
oh003	276	40	treering	0.40	-0.83	288	-35	1	1	Yes
oh006	279	40	treering	0.40	-0.90	325	-48	1	1	Yes
ok001	265	37	treering	0.40	-1.07	275	-29	1	1	Yes
ok004	264	37	treering	0.40	-1.07	213	-29	1	1	Yes
ok007	264	36	treering	0.40	-1.07	339	-45	1	1	Yes
ok013	262	36	treering	0.40	-1.37	270	-29	1	1	Yes
ok016	264	35	treering	0.40	-1.07	205	-29	1	1	Yes
ok019	265	34	treering	0.40	-1.63	326	-29	1	1	Yes
ok025	262	34	treering	0.40	-1.99	259	-45	1	1	Yes
ok028	261	35	treering	0.40	-1.99	264	-29	1	1	Yes
ok031	265	34	treering	0.40	-1.63	265	-32	1	1	Yes
Oppo et al. (2009) SST	119	-5	marine	0.40	-0.38	1925	-5	11	50	Yes
or040	242	46	treering	0.40	0.25	275	-41	1	1	Yes
pa001	282	41	treering	0.40	-0.75	341	-31	1	1	Yes
pa005	280	40	treering	0.40	-0.90	327	-31	1	1	Yes
pa007	282	40	treering	0.40	-0.75	415	-31	1	1	Yes

Table 2 continued from previous page

Reference	Lon	Lat	Proxy	SNR	EOF	Start	End	Res	Dating	Included?
pa009	284	40	treering	0.40	-0.75	319	-31	1	1	Yes
pa012	282	40	treering	0.40	-0.75	338	-31	1	1	Yes
Powers et al. (2011)	34	-10	lake	N/A	N/A	667	-46	41	50	No; AOI
Quinn et al. (1998)	167	-23	coral	0.33	-2.06	292	-43	1	1	Yes
Quinn et al. (2006) $\delta^{18}O$	152	4	coral	N/A	N/A	83	-48	1	1	No; Length
Richey et al. (2009) Fisk	268	28	marine	0.40	-1.33	702	-50	19	35	Yes
Richey et al. (2009) Garrison	266	27	marine	0.40	-1.64	529	-50	33	45	Yes
Saenger et al. (2009) ext	281	26	coral	0.73	-0.14	398	-41	1	1	Yes
Saenger et al. (2011) ggc	284	33	marine	0.40	-1.22	1500	100	100	45	Yes
Saenger et al. (2011) mc	284	33	marine	0.40	-1.22	1700	100	100	40	Yes
spai009	358	40	treering	0.40	0.23	262	-38	1	1	Yes
spai011	358	40	treering	0.40	0.23	465	-38	1	1	Yes
spai013	0	40	treering	0.40	-0.18	265	-42	1	1	Yes
spai016	355	41	treering	0.40	0.23	283	-38	1	1	Yes
spai018	355	40	treering	0.40	0.23	263	-39	1	1	Yes
spai019	356	41	treering	0.40	0.23	427	-38	1	1	Yes
spai029	358	40	treering	0.40	0.23	239	-33	1	1	Yes
spai036	356	41	treering	0.40	0.23	201	-33	1	1	Yes
spai037	356	41	treering	0.40	0.23	289	-35	1	1	Yes
spai038	356	41	treering	0.40	0.23	351	-34	1	1	Yes
spai041	1	40	treering	0.40	-0.18	269	-35	1	1	Yes
spai045	358	40	treering	0.40	0.23	312	-35	1	1	Yes
spai046	358	40	treering	0.40	0.23	306	-35	1	1	Yes
Stott et al. (2002) *G.Ruber*	126	6	marine	0.40	-0.46	67592	89	25	50	Yes
Sundqvist et al. (2013)	29	-24	speleothem	0.46	0.45	315	-43	1	3	Yes
Thompson et al. (1995)	282	-9	ice core	0.40	0.92	19100	0	100	20	Yes
Thompson and et Al. (1997)	82	35	ice core	0.40	-0.13	1946	-34	10	20	Yes
Thompson et al. (2002) furt	37	-3	ice core	0.40	0.62	270	30	10	20	Yes
Thompson et al. (2002) knif2	37	-3	ice core	0.40	0.62	1490	0	10	20	Yes
Thompson et al. (2002) knif3	37	-3	ice core	0.40	0.62	1490	0	10	20	Yes
Thompson et al. (2002) ksif1	37	-3	ice core	0.40	0.62	1270	0	10	20	Yes
Thompson et al. (2002) ksif2	37	-3	ice core	0.40	0.62	1470	0	10	20	Yes
Thompson et al. (2003) Dasuopu	86	28	ice core	0.40	-0.07	940	-47	10	20	Yes
Thompson et al. (2003) Dunde	96	38	ice core	0.40	0.14	940	-37	10	20	Yes
Thompson et al. (2006) c1 $\delta^{18}O$	89	34	ice core	N/A	N/A	1946	-44	5	95	No; Dating error
Thompson et al. (2006) c2 $\delta^{18}O$	89	34	ice core	0.40	-0.66	1946	-44	5	50	Yes

Reference	Lon	Lat	Proxy	SNR	EOF	Start	End	Res	Dating	Included?
Table 2 continued from previous page										
Thompson et al. (2006) Dunde an	96	38	ice core	0.40	0.14	344	-31	5	20	Yes
Thompson et al. (2006) Dunde $\delta^{18}O$	96	38	ice core	0.40	0.14	1426	-32	10	20	Yes
Thompson et al. (2013) nd	289	-14	ice core	0.40	0.43	945	-45	10	10	Yes
Thompson et al. (2013) sd	289	-14	ice core	0.66	0.43	1724	-59	1	10	Yes
Tierney et al. (2015) bc1 SST	44	45	marine	0.40	-0.69	322	-50	9	25	Yes
Tierney et al. (2015) p SST	44	45	marine	0.40	-0.69	1819	-30	20	25	Yes
Tiwari et al. (2015)	74	13	marine	0.40	0.11	4772	154	62	45	Yes
tn008	276	36	treering	0.40	-1.12	317	-30	1	1	Yes
Tudhope et al. (2001) Laing	145	-4	coral	N/A	N/A	65	-43	1	1	No; Length
Tudhope et al. (2001) Madang	146	-5	coral	N/A	N/A	69	-43	1	1	No; Length
turk001	31	40	treering	0.40	-1.23	658	-51	1	1	Yes
turk005	30	37	treering	0.40	-1.13	580	-38	1	1	Yes
turk006	30	37	treering	0.40	-1.13	590	-38	1	1	Yes
ut013	250	41	treering	0.40	0.73	517	-21	1	1	Yes
ut018	251	39	treering	0.40	0.73	461	-22	1	1	Yes
ut020	250	38	treering	0.40	0.42	505	-21	1	1	Yes
ut021	249	37	treering	0.40	0.42	385	-21	1	1	Yes
ut023	250	38	treering	0.40	0.42	603	-22	1	1	Yes
ut024	250	38	treering	0.40	0.42	674	-20	1	1	Yes
ut501	250	41	treering	0.40	0.73	315	-21	1	1	Yes
va008	281	38	treering	0.40	-0.90	290	-28	1	1	Yes
va009	281	38	treering	0.40	-1.09	363	-32	1	1	Yes
va010	281	38	treering	0.40	-1.09	419	-32	1	1	Yes
va012	278	37	treering	0.40	-1.09	305	-32	1	1	Yes
van Hengstum et al. (2015) whc4	295	32	marine	0.40	-0.77	2792	-56	30	35	Yes
Vasquez-Bedoya et al. (2012) ext	273	21	coral	1.04	-0.20	177	-59	1	1	Yes
wa048	238	47	treering	0.40	0.40	664	-29	1	1	Yes
wa056	239	47	treering	0.40	0.40	691	-29	1	1	Yes
wa057	239	48	treering	0.40	0.40	520	-30	1	1	Yes
wa058	237	48	treering	0.40	0.40	533	-30	1	1	Yes
wa063	239	47	treering	0.40	0.40	364	-30	1	1	Yes
wa065	239	48	treering	0.40	0.40	408	-32	1	1	Yes
wa085	239	47	treering	0.40	0.40	435	-37	1	1	Yes
Wörheide (1998)	146	-15	coral	0.40	-0.96	398	-40	10	10	Yes
Wu et al. (2013) Sr/Ca	186	-20	coral	N/A	N/A	159	-53	1	1	No; AOI
Wurtzel et al. (2013)	295	11	marine	0.40	0.89	2010	-58	1	60	Yes
Table 2 continued on next page										

1465

Table 2 continued from previous page										
Reference	Lon	Lat	Proxy	SNR	EOF	Start	End	Res	Dating	Included?
wv002	281	39	treering	0.40	-0.90	440	-29	1	1	Yes
Zhao et al. (2000)	240	34	marine	0.40	1.05	653	9	1	5	Yes
Zinke et al. (2014) AC	44	-23	coral	0.40	0.00	290	-44	1	1	Yes
Zinke et al. (2014) HAI	114	-29	coral	0.88	-0.46	155	-60	1	1	Yes
Zinke et al. (2015) Ning	114	-22	coral	N/A	N/A	71	-58	1	1	No; Length
Zinke et al. (2015) Rowley	119	-17	coral	0.63	-0.63	152	-59	1	1	Yes

Table 2. Precipitation proxy details. 'SNR' gives the signal-to-noise ratio used to make the pseudoproxies. 'EOF' gives the (unscaled) 20CRV2c EOF value used to weight the proxy. 'Start' and 'End' are starting and ending years in YearBP. 'Res' is proxy resolution, rounded to the nearest integer; sub-annual proxies are listed as having a 1-year resolution. 'Dating' refers to dating error. 'Included?' indicates whether the proxy contributed to the final ENSO reconstruction; if not, the reason for exclusion is listed ('Dating error' and 'Length' are *a priori* conditions which the proxies failed to meet. 'AOI' indicates it passed pre-processing screening, but was not selected during the add-one-in process).